Modeling of plasma-based CO_2 conversion : lumping of the vibrational levels

Reference:

Berthelot Antonin, Bogaerts Annemie.- Modeling of plasma-based CO_2 conversion : lumping of the vibrational levels
Plasma sources science and technology / Institute of Physics - ISSN 0963-0252 - 25:4(2016), 045022
Full text (Publishers DOI): http://dx.doi.org/doi:10.1088/0963-0252/25/4/045022

Modeling of plasma-based CO_2 conversion: lumping of the vibrational levels

Antonin Berthelot and Annemie Bogaerts

Department of Chemistry, Research group PLASMANT, University of Antwerp, Universiteitsplein 1, 2610 Antwerp, Belgium

E-mail: antonin.berthelot@uantwerpen.be

Abstract. Although CO_2 conversion by plasma technology is gaining increasing interest, the underlying mechanisms for an energy-efficient process are still far from understood. In this work, a reduced non-equilibrium CO_2 plasma chemistry set, based on level lumping of the vibrational levels, is proposed and the reliability of this level-lumping method is tested by a self-consistent zero-dimensional code. A severe reduction of the number of equations to be solved is achieved, which is crucial to be able to model non-equilibrium CO_2 plasmas by 2-dimensional models. Typical conditions of pressure and power used in a microwave plasma for CO_2 conversion are investigated. Several different sets, using different numbers of lumped groups, are considered. The lumped models with 1, 2 or 3 groups are able to reproduce the gas temperature, electron density and electron temperature profiles, as calculated by the full model treating all individual excited levels, in the entire pressure range investigated. Furthermore, a 3-groups model is also able to reproduce the shape of the vibrational distribution function (VDF) and gives the most reliable prediction of the CO_2 conversion. A strong influence of the vibrational excitation on the plasma characteristics is observed. Finally, the limitations of the lumped-levels method are discussed.

Keywords: CO_2 conversion, microwave, chemistry reduction, lumped-levels

Submitted to: *Plasma Sources Sci. Technol.*

1. Introduction

There has been a growing interest for CO_2 conversion over the last few years, due to the increase of the greenhouse gas concentration in the atmosphere[1]. CO_2 conversion into CO has been proven to be very efficient using microwave plasma discharges [2]. An energy efficiency of about 90% was found in conditions of supersonic gas flow [3]. More recently, new studies have been carried out to evaluate the potential industrial applications of CO_2 dissociation using microwave discharges [4, 5, 6, 7, 8]. To our knowledge, the best energy efficiencies currently reported at atmospheric pressure are between 40 and 50 % [8]. This high energy efficiency is attributed to the excitation of the asymmetric vibrational mode of CO_2, which has been shown to be a very efficient

way to enhance the dissociation, even at low gas temperatures[9, 10]. A large number of processes among vibrational levels, such as vibrational-vibrational (VV) and vibrational-translational (VT) relaxation, needs to be taken into account in order to understand the different conversion mechanisms taking place in such a discharge.

In order to describe these processes, a large chemistry set for CO_2 dissociation has been developed in our group [9, 10]. The number of species that needs to be taken into account in a state-to-state non-equilibrium CO_2 plasma model is very large and this makes such a model computationally expensive. Indeed, the vibrational excitation plays an important role in the efficient dissociation of CO_2 [2] and an accurate description of the Vibrational Distribution Function (VDF) is needed. That is why most of the numerical studies done so far on the subject have been limited to 0D-models[9, 10, 11, 12, 13, 14]. However, some processes cannot be accurately included in a 0D-model and strong approximations on the geometry and the diffusion processes need to be made. In order to model a discharge in more dimensions, it is necessary to considerably reduce the chemistry set with as little losses of accuracy as possible in the predictions of the model.

The Principal Component Analysis (PCA) method has been used [15] to reveal the underlying manifolds present in the plasma chemistry of CO_2. It was shown that using only two principal components, this method allows to accurately reproduce the entire chemistry of the CO_2 plasma. However, this method has not been implemented yet in a self-consistent plasma code and its use in an existing code can be complex due to the use of large-dimensional lookup-tables for the source terms, as well as the instabilities that can arise.

Therefore, we have decided to apply a different strategy to reduce the number of equations to be solved in the model, i.e., the lumping of the vibrationally excited levels. In [16], a method to reduce the complexity of a collisional radiative model has been developed in the case of atomic hydrogen, comparing two grouping strategies: uniform and Boltzmann groups. It was shown that the Boltzmann approach using different internal temperatures gives better results. In [17, 18], a multi-internal temperature model is derived for the vibrational levels of N_2 and electronic levels of N in hypersonic nitrogen flows. A good agreement was observed between the multi-internal temperature model and the detailed model considering individual levels. However, to our knowledge, such a level lumping method has not yet been applied for CO_2.

In this work, before applying the level-lumping, we first reduce the complexity and the number of species included in the chemistry set from our previous work [9, 10] . Subsequently, a lumped-model is proposed to describe the VDF using fewer variables, thus making this chemistry set compatible with 2D or 3D models. In section 2, we describe the self-consistent 0D model that was used to reduce the chemistry set and to test the accuracy of the level lumping strategy. We also present the reduced chemistry set and we introduce the equations used to describe the different groups in the lumped model. In section 3, first, a comparison between the predictions given by the two chemistry sets is shown, followed by a comparison of the models considering

the individual vibrational levels and the grouped-levels (with a different number of groups), for different conditions of pressure and power, and for fixed or self-consistently calculated gas temperature. The effect of the description of the VDF on the other plasma parameters is also shown, stressing the importance of an accurate description of the VDF in a self-consistent CO_2 plasma model. Finally, the limitations of the level-lumping strategy proposed here will be discussed.

2. Model description

2.1. Discharge geometry and conditions

A 0D model only allows us to model simple reactors, such as the surfatron [19] setup presented in [6]. It consists of a quartz discharge tube and a waveguide bringing the microwaves perpendicular to the tube, forming a plasma. The plasma also has an effect on the propagation of the electromagnetic waves and a self-consistent model including the description of the microwave fields would require going to higher dimensions.

In this model, we follow a volume moving through the discharge tube at a velocity

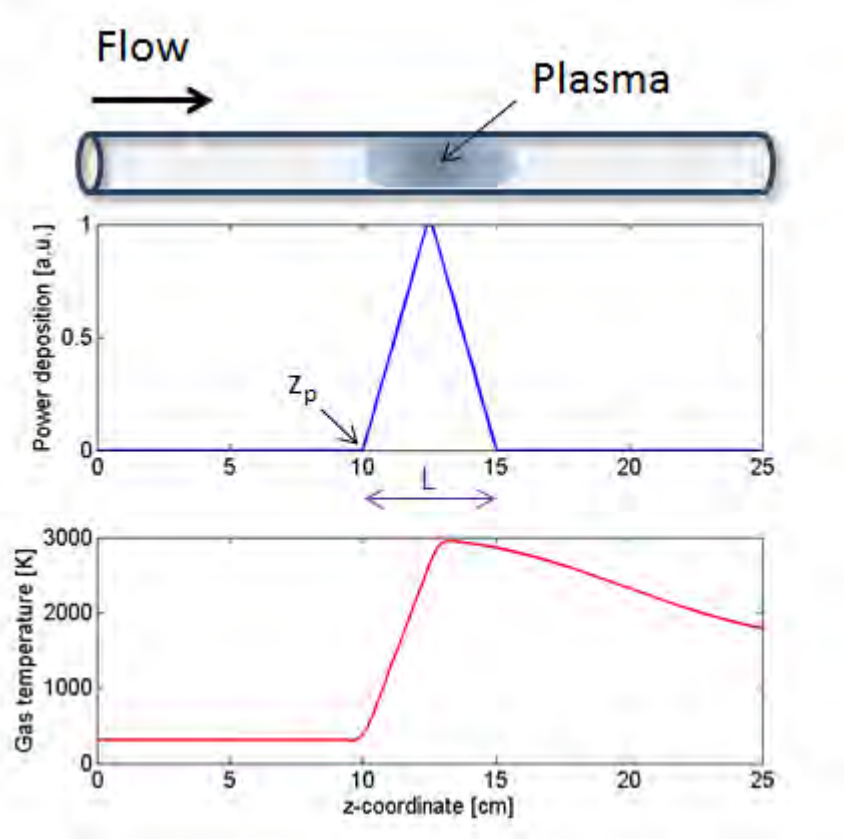

Figure 1. Schematic description of the geometry (upper panel), shape of the power deposition profile (middle panel) and typical gas temperature profile(lower panel).

v defined as:

$$v = \frac{\mathcal{Q}_m}{\rho \mathcal{A}} \tag{1}$$

where $\mathcal{Q}_m$ is the mass flow rate, $\mathcal{A} = \pi * R^2$ is the discharge tube cross-section area (R = 9mm) and $\rho = \sum_s n_s M_s$ is the gas mass density. Although we solve the species densities and electron mean energy as a function of time in the 0D model, this time can be translated to an axial position (coordinate z) in the reactor, by means of the gas velocity. The direction of the flow is shown in Figure 1. The shape of the microwave power deposition Q_{MW} can then be presented as a function of the axial position, according to theoretical calculations [20] and is also shown in Figure 1. The absolute value of Q_{MW} is determined by solving:

$$P = \mathcal{A} \int_{z_p}^{z_p+L} Q_{MW}(z)\, \mathrm{d}z = \frac{\mathcal{A}L}{2} Q_{MW,max} \tag{2}$$

Where P is the total microwave deposited power, $Q_{MW,max}$ is the maximum value of the local microwave power deposition, z_p is the axial position where the plasma starts and L is the plasma length, as shown in figure 1.

Indeed, the MW plasma under study can be considered as a plug flow reactor. Due to the equivalence of a plug flow reactor (where the variables change as a function of position in the tube) and a batch reactor (where the variables change only as a function of time), we can model our MW plasma with a 0D model, describing the evolution of the species densities and electron mean energy as a function of time, which corresponds to a given residence time in the reactor, but also to a given position in the reactor. This time can indeed be translated to an axial position, by means of the gas velocity.

A self-consistently calculated gas temperature is used in section 3.3, but in section 3.1 and 3.2, we consider a fixed temperature profile, increasing from 300K to 3000K in the plasma as shown in figure 1. The maximum value of T_g=3000K, as well as the shape, are based on the predictions by our self-consistent model (see section 3.3 below). The shape of the temperature profile is also similar to the typical shape obtained by 2D models of similar discharges [21]. The use of a temperature profile in section 3.2 instead of a self-consistent calculation is motivated by the strong influence of the VDF on the gas temperature (see section 3.3) and vice-versa. Thus, by applying a fixed temperature profile, this allows us, in a first step, to analyse the ability of the lumped-levels models to accurately describe the VDF for a given temperature.

Note that the use of this configuration, shown in figure 1, is not motivated by the description of a particular experiment. Instead, the parameters are chosen as typical conditions studied for CO_2 dissociation by microwave plasma, as the set needs to be tested for realistic conditions.

2.2. Description of the equations solved

A zero-dimensional chemical kinetics model was developed using the commercial software COMSOL Multiphysics to simulate the plasma chemistry of a CO_2 non-

equilibrium plasma. The densities of the different species are solved following equation 3:

$$\frac{dn_s}{dt} = \sum_j \left[(a_{sj}^R - a_{sj}^L) R_j \right] \tag{3}$$

where n_s is the density of the species s, a_{sj}^R and a_{sj}^L are the right and left-hand stoichiometric coefficients of species s in the reaction j, respectively, and R_j is the reaction rate defined as:

$$R_j = k_j \prod_l n_l \tag{4}$$

k_j is the rate coefficient of reaction j, and n_l stands for the density of the various reactants l in this reaction. Furthermore, a conservation equation is solved for the mean electron energy:

$$\frac{dn_e\overline{\epsilon_e}}{dt} = Q_{MW} - \sum_s \frac{3}{2} n_e \nu_{ms} k_B \frac{2m_e}{M_s}(T_e - T_g) + \sum_j n_e k_j n_j \Delta\epsilon_j \tag{5}$$

where n_e is the electron density, $\overline{\epsilon_e}$ is the mean electron energy, Q_{MW} is the microwave heating source term, ν_{ms} is the electron momentum transfer frequency with species s, m_e is the electron mass, M_s is the mass of species s, T_e and T_g are the electron temperature and the gas translational temperature, respectively, and $\Delta\epsilon_j$ is the change in electron energy caused by electron-impact reaction with species j (whose density is indicated as n_j). Note that the model solves the logarithm of the species densities n_s and electron energy density $n_e\overline{\epsilon_e}$, in order to improve the stability of the simulation. The electron temperature is then obtained from $T_e = \frac{2}{3}\overline{\epsilon_e}$.

All the other plasma species besides the electrons, i.e. the various molecules, radicals and ions, also called the "heavy species", are assumed to have the same translational temperature T_g. This temperature is either given as an input of the model or self-consistently calculated using:

$$N\frac{\gamma k_B}{\gamma - 1}\frac{dT_g}{dt} = P_{e,el} - \sum_j R_j \Delta H_j \tag{6}$$

where $N = \frac{p}{k_B T_g} = \sum_s n_s$ is the total gas density (i.e., the sum of the number densities of all heavy species), p is the pressure, $P_{e,el}$ is the power transferred from the electrons to the heavy particles by elastic collisions, corresponding to the second term of the right-hand side of equation 5. ΔH_j is the heat released or consumed in the reaction j. $\gamma = \frac{C_p}{C_v}$, the specific heat ratio, is the ratio between the heat capacity per unit mass at constant pressure C_p and at constant volume C_v. Note that this expression neglects the heat losses by conduction and by radiation. While this is an approximation in some of the cases studied here, the goal of this study is to assess the effect of the level-lumping strategy on the results of the model and not to model a specific experiment. γ is here defined as:

$$N\frac{\gamma}{\gamma - 1} = \sum_s n_s \frac{\gamma_s}{\gamma_s - 1} \tag{7}$$

Temperature	300-1200K	1200-3000K
A	369.4	1327
B	1845	-53.85
C	-1429	31.52
D	401.2	-5.841
E	3.664	-109.6

Table 1. Coefficients in [J.kg^{-1}.K^{-1}] for calculating the specific heat capacity C_p of CO_2 in equation 8

where γ_s is the specific heat ratio of species s.

As in the previous work from our group [10], the specific heat ratio is here 1.67 for atomic species and 1.40 for diatomic molecules. For CO_2, we only have to take into account the heat capacity due to translational and rotational degrees of freedom, as well as the vibrational symmetric mode levels that are not described by an individual species (see below). C_p can be expressed as in [10].

$$C_p = A + Bt + Ct^2 + Dt^3 + Et^{-2} \tag{8}$$

Where $t = T/1000[K]$. The coefficients A, B, C, D and E are shown in table 1. We then use $\gamma_s = (1 - \frac{k_b}{C_p M_s})^{-1}$ to obtain γ_{CO_2}[10].

2.3. Reduction of the chemistry set

The chemistry set developed by [9, 10], which will be referred to as "full set", is in a first step simplified by removing all the species that do not significantly contribute to the plasma chemistry. In order to determine which are the main species and processes to take into account, the model of [9, 10] was implemented in ZDPlaskin [22]. Simulations are performed for a gas flow rate of 3slm and a microwave power of 500W, yielding a specific energy input (SEI) of 2.3eV/molec. The gas temperature profile shown in figure 1 is used. A comparison of the predictions given by the full and the reduced chemistry sets obtained in this way is given below in section 3. The list of species that are considered in the reduced model is shown in table 2. The list of species removed from the full set is shown in Appendix B (table B1). Note that no excited states have been kept for CO and only 3 vibrational levels have been kept at pressures of 200mbar and above for O_2. The influence of the states removed from the full set was found to be negligible at these conditions, due to the relatively low number densities of CO and O_2 (see figure 4 below). In cases where their number densities are higher, i.e. when the conversion is larger, the contribution of these electronically excited levels may not be negligible anymore, so in this case, the full chemistry set, or a reduced set with more species, should be used.

The list of the different reactions considered in the reduced set is shown in Appendix A (tables A1, A2,A3 and A4).

Table 2. Species described in the model.

Neutral ground states
CO_2, CO, O_2, O, C

Charged species
CO_2^+, CO_3^-, O^-, O_2^-, e^-

Excited states	Associated energy [eV]	State
[a]$O_2[v_{1-3}]$	0.19 eV, 0.38 eV & 0.57 eV[23]	
$CO_2[v_{1-21}]$	Anharmonic oscillator[24]	(00n)
$CO_2[v_a]$	0.083 eV	(010)
$CO_2[v_b]$	0.167 eV	(020) + (100)
$CO_2[v_c]$	0.252 eV	(030) + (110)
$CO_2[v_d]$	0.339 eV	(040) + (120) + (200)
CO_2^*	6.23 eV	$(^1\Pi_g)$

[a] The three levels $O_2[v_{1-3}]$ have only been considered for pressures of 200mbar and above.

2.4. Level lumping

The reduced model presented above is further reduced by grouping the asymmetric mode vibrational levels ($CO_2[v_{1-21}]$ in Table 2) into l lumped levels. The symmetric mode vibrational levels (i.e., CO_2 [v_a, v_b, v_c, v_d] in Table 2) are not further lumped together. The lumping of the asymmetric mode vibrational levels is realized by introducing n_{g_i}, the total number density of all the levels j within one lumped level i.

$$n_{g_i} = \sum_{j \in g_i} n_j \qquad i = 1, ..., l \tag{9}$$

It is then necessary to describe the distribution of the levels within the group g_i using a function $f(E_j, T_i)$, where E_j is the energy of the j^{th} level within group g_i, and T_i is the temperature associated to the group g_i.

$$n_{j \in g_i} = n_{g_i} \frac{f(E_j, T_i)}{\sum\limits_{j \in g_i} f(E_j, T_i)} \tag{10}$$

In the case of a Maxwellian internal vibrational distribution where all the levels have the same degeneracy, this gives:

$$n_{j \in g_i} = \frac{n_{g_i} exp(-\frac{E_j}{k_b.T_i})}{\sum\limits_{j \in g_i} exp(-\frac{E_j}{k_b.T_i})} \tag{11}$$

Since the VDF is typically not a Maxwelian distribution, we recommend to use several groups when the VDF cannot be known in advance. In the case the user knows which

VDF to expect, different inner-distribution functions can be chosen in order to limit the number of groups to be used. However, this limits the applicability of the method. Therefore, when the VDF is not known, the use of several groups, as presented here, makes the method more generally applicable.

In order to solve for the density of the group instead of the density of each individual level, we need to re-define the conservation equation 3:

$$\frac{dn_{g_i}}{dt} = \sum_{j \in g_i} \frac{dn_j}{dt} = \sum_{j \in g_i} S_j \tag{12}$$

where S_j is the source term for each individual level j, i.e. the right-hand side of equation 3. Additionally, for each group, another conservation equation is required to describe the inner-distribution within each group. In this work, we have chosen to solve for the mean group vibrational energy:

$$\overline{E_{g_i}} = \frac{1}{n_{g_i}} \sum_{j \in g_i} E_j n_j \tag{13}$$

where E_j is the energy associated to each vibrational level, obtained from the anharmonic oscillator approximation [24]. We can then define a conservation equation for $\overline{E_{g_i}}$, by taking the time-derivative of equation 13 and using equation 12:

$$\frac{d\overline{E_{g_i}}}{dt} = \frac{\sum\limits_{j \in g_i} E_j S_j - \overline{E_{g_i}} \sum\limits_{j \in g_i} S_j}{n_{g_i}} \tag{14}$$

Note that instead of solving for $\overline{E_{g_i}}$ other choices are also possible, such as solving for the density of one level within the group [16].

Obtaining the distribution of the levels within each group, based on a Boltzmann distribution, requires to know the temperatures T_i, as shown in equations 10 and 11. However, the model solves for the mean group energy $\overline{E_{g_i}}$. Therefore, for each group considered in the model, we need to use lookup-tables giving T_i as a function of $\overline{E_{g_i}}$. The relation between T_i and $\overline{E_{g_i}}$ is established by equation 15.

$$\overline{E_{g_i}} = \frac{\sum\limits_{j \in g_i} E_j exp(-\frac{E_j}{k_b.T_i})}{\sum\limits_{j \in g_i} exp(-\frac{E_j}{k_b.T_i})} \tag{15}$$

Alternatively to the level lumping strategy, one can assume thermal equilibrium between the vibrational temperature and the gas translational temperature, which gives the following description of the VDF:

$$n_k = \frac{n_0 exp(-\frac{E_k}{k_b.T_g})}{\sum\limits_{0 \leq j \leq 21} exp(-\frac{E_j}{k_b.T_g})} \qquad k = 1, ..., 21 \tag{16}$$

This will be referred to as 'thermal distribution model' in the following. n_0 refers to the density of the CO_2 ground state.

This level-lumping method is developed with the Comsol Multiphysics code. In this code, the rate coefficients of the electron impact reactions are calculated by means

of an external Boltzmann solver, i.e., Bolsig+ [25]. The latter calculates the Electron Energy Distribution Function (EEDF) for given values of mean energy, based on all electron impact reactions included in the model. This is a necessary approximation, as a 2D-model solving the Boltzmann equation would be computationally expensive. For additional information, the effect of the vibrational collisions and the superelastic collisions on the EEDF is discussed in [12].

The system of equations described above is solved using a Newton iterative procedure and the direct solver MUMPS, both coded in the Comsol Multiphysics software.

3. Results and discussion

As mentioned above, the first step of this study is the simplification of the chemistry set previously used, by identifying the main chemical processes taking place in this kind of discharge. We assess the validity of the reduced chemistry set over a range of pressures commonly used in the experiments (from 20 mbar to atmospheric pressure)[6, 2, 8].

In section 3.1, we present a comparison of the model predictions using the full and the reduced chemistry set for the main model outputs: CO_2 conversion, VDF, electron temperature and density.

In section 3.2, we show the influence of the number of lumped levels (or groups) considered in the level-lumping strategy on the accuracy of the description of the VDF. This is done using the temperature profile shown in figure 1 in order to leave out the effects of the gas temperature on the VDF and to focus on the predictions of the VDF given by the lumped-levels model.

In section 3.3, the most important plasma quantities, calculated with the various lumped-levels models using the self-consistent gas translational temperature calculation, will be compared to assess the validity of the lumped-level strategy

Finally, in section 3.4, we discuss the limitations of the lumped-levels model and its range of applicability.

Table 3 shows the levels included within each group, for each of the lumped-levels models developed, i.e., one-group (1G), two-groups (2G) and three-groups (3G) model. This levels-repartition was chosen in order to fit the VDF predicted by the individual-levels model. The same groups are considered for all the conditions investigated in order to make the lumped-levels models as general as possible. We use a Boltzmann distribution to describe the distribution of levels within each group. However, this does not assume that the entire VDF follows a Boltzmann distribution, as the 2-groups and 3-groups models assume a different vibrational temperature for each group.

Finally, we will also study the effect of assuming simply a thermal vibrational distribution (as defined by the gas temperature), as well as no vibrational distribution of the asymmetric mode at all.

	Group 1	Group 2	Group 3
1G model	1-21	×	×
2G model	1-3	4-21	×
3G model	1-3	4-14	15-21

Table 3. Asymmetric mode vibrational levels included within each group, for the different lumped-levels models developed

The definition of CO_2 conversion is given by equation 17.

$$X = 1 - \frac{v(z_{out})n_{CO_2,tot}(z_{out})}{v(z_0)n_{CO_2,tot}(z_0)} \tag{17}$$

where v is the gas velocity, z_{out} is the outlet axial position, and z_0 is the inlet axial position.

3.1. Reduction of the chemistry set

This section discusses the effects of the first chemistry reduction performed on the set of [9, 10] and assesses its validity. Table 4 shows the predicted CO_2 conversion for different pressures. It is clear that the consequences of the reduction of the chemistry set on the calculated CO_2 conversion in these conditions are small, especially considering the magnitude of the chemistry reduction, i.e., from 126 species to 36 or 39 depending on the pressure. The chemistry set could indeed be reduced to 36 species at a pressure of 100 mbar and below, while at 200 mbar and above, 39 species have to be considered. At these higher pressures, the 3 vibrational levels of O_2 are necessary in the reduced chemistry set to keep the difference in calculated CO_2 conversion below 5 %. Their role is found to be less important at 100 mbar and below. Keeping in mind the balance between accuracy and computational load, we judged it unnecessary to keep the 3 vibrational levels of O_2 at pressures of 100mbar and below. At higher pressure, their presence enhances the recombination reaction of CO in CO_2 (i.e. N4 in table A4), due to the lower activation energy of this reaction for a vibrationally excited state of O_2, thus affecting the calculated CO_2 conversion. This explains why the difference in predicted CO_2 conversion between the full set and the reduced set is larger at 100mbar than at 200mbar: the vibrational levels of O_2 still have a minor effect on the CO_2 conversion at 100mbar and removing them slightly increases the error.

Figure 2 shows the comparison of the VDF predicted by the full and the reduced chemistry sets, both in the plasma and in the afterglow at 20 mbar, 100 mbar and 1 bar. At 20 mbar, the reduced set predicts a slightly underestimated density in the plasma for the last three vibrational levels. At 1 bar, the reduced set slightly overestimates the last two levels in the plasma. However, the VDFs determined by the reduced set are overall in very good agreement with the VDFs predicted by the full set, in the entire range of pressures investigated, both in the plasma and in the afterglow. As the reduced chemistry set does not account for the CO vibrational levels, in contrast to the

CO_2 conversion	Reduced set	Full set	Relative difference
20 mbar	1.01 %	1.0 %	1.1 %
100 mbar	15.3 %	14.9 %	2.6 %
200 mbar	26.8 %	26.6 %	0.7 %
500 mbar	11.7 %	11.5 %	1.2 %
1 bar	5.01 %	4.96 %	1.2 %

Table 4. Comparison of the CO_2 conversion predicted by the full and the reduced chemistry sets at five different pressures and a SEI of 2.3 eV/molec

full chemistry set, which considers 63 CO vibrational levels, this shows that, under these conditions, the contribution of the CO vibrational level population to the CO_2 VDF is negligible. Not taking them into account only has a minor influence. A more detailed description of the VDF will be given in the next section.

In the full model, various positive ions were included, but the role of the individual ions in the actual CO_2 conversion is minor, both directly and indirectly (through determining the electron density). Therefore, in the reduced model, only 1 type of positive ion is kept, i.e., CO_2^+. Figure 3 shows a comparison between the full model and the reduced model for the total positive ion density, the densities of the two major negative ions, i.e., CO_3^- and O^-, and the electron density, at 20 mbar, 100 mbar and 1 bar.

At 20mbar, the model using the full set predicts a fast rise of the electron density at the beginning of the plasma (z=10cm). The electron density keeps rising until z=12cm and then drops. In the afterglow (z>15cm), the electron density drops slowly and has values in the order of 10^{15} m^{-3}. The model with the reduced chemistry set predicts the same rise, but a faster drop in the electron density, so that the maximum electron density is lower, and reached at an earlier position, than in case of the full set. This will be explained below.

At 100 mbar and 1 bar, the model with the full set also predicts a fast rise of the electron density at the beginning of the plasma (z=10cm), but the maximum is reached at a somewhat later position (z=12.5cm), and the density initially also drops more slowly than at 20mbar, but at the end of the plasma it drops rapidly. In the afterglow (z>15cm), the electron density drops slowly at 100mbar, and has values in the order of 10^{14} m^{-3}, while at 1bar, the electron density drops faster and quickly reaches low values, in the order of 10^{13} m^{-3}. The model with the reduced set predicts the same electron density profiles at both 100 mbar and 1 bar.

As observed in figure 3 (a), the agreement between full set and reduced set is not so good at 20mbar. This is attributed to the removal of several ions in the reduced set, which has a considerable effect on the electron density at this pressure. However, the overall CO_2 conversion calculated by the reduced and full set is still in good agreement at 20mbar. This can be explained by the importance of thermal dissociation when using the gas temperature profile plotted in figure 1, making the electron excitation of the

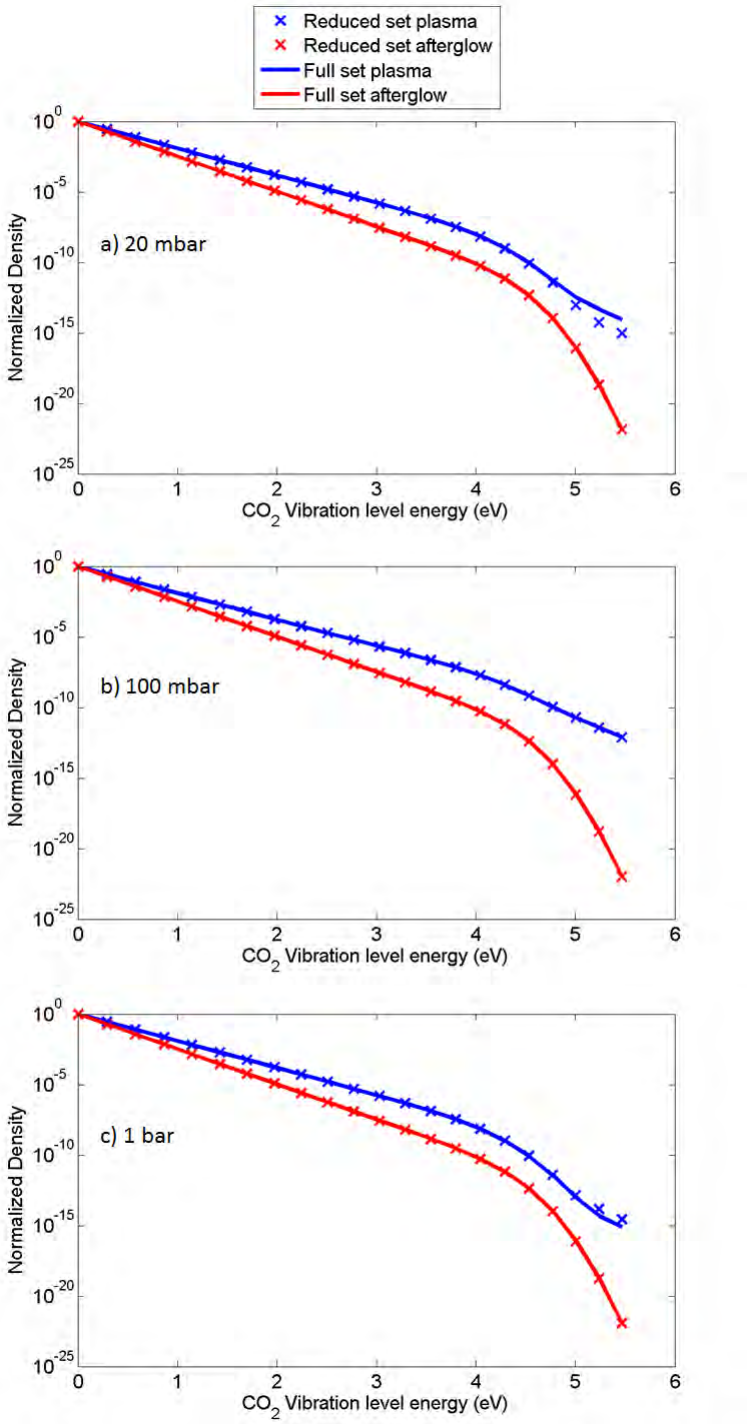

Figure 2. Comparison of the VDFs predicted in the plasma (blue) at z=12.5cm and in the afterglow (red) at z=22.5cm, by the full chemistry set (lines) and the reduced set (crosses), at p=20 mbar, 100mbar and 1bar and a SEI of 2.3 eV/molec

vibrational levels less important at this pressure. At 100mbar and 1bar, the agreement for the electron density is much better.

At 20mbar, the total positive ions density is much lower with the reduced set than with the full set from z=11.5cm. Consequently, the electron density and also the negative ion densities are lower. At 100mbar, the agreement between the different ion densities is almost perfect. The removal of several ions thus has only very little effect on the charged particles kinetics at this pressure. At 1bar, from z=10.5cm to z=12.5cm, the reduced set underestimates the density of both positive and negative ions. However, the difference between them, giving the electron density, remains very close to what is predicted by the full set. In the rest of the simulation region, a very good agreement between the different charged particle densities is reached. Most of the applications of CO_2 conversion using microwave plasma use pressures of 100mbar or more[26]. Moreover, the ions have very little direct effect on the CO_2 conversion and are therefore only important for the determination of the electron density. That is why we did not judge it necessary to keep more ions in the reduced chemistry set.

Figure 4 illustrates the axial density profiles of CO, CO_2, O and O_2 calculated by the full and the reduced sets at p=20 mbar, 100 mbar and 1bar. At 20 mbar and 100 mbar, since the conversion remains rather low (less than 20 %, see table 4), the CO_2 profile follows more or less the inverse of the gas temperature profile. Indeed, the model ensures that the densities comply with the ideal gas law. At 1 bar, we see an additional drop in the CO_2 density around z=13cm, which is explained by the large local conversion of CO_2 at this position. However, due to the recombination of CO with O and O_2, the density of CO_2 increases again later, explaining the rather low overall conversion.

In all three cases, the CO density greatly increases in the plasma, as a result of the CO_2 conversion. At 100 mbar, it stays constant in the afterglow (i.e. $z > 15$ cm), while it keeps on increasing slightly at 20 mbar due to the thermal conversion of CO_2 and it decreases at 1 bar due to the recombination of CO with O, mentioned above.

The O and O_2 density profiles follow more or less the CO density profiles at all pressures, since they all originate from the CO_2 dissociation. Nevertheless, the O density is found to be higher than the O_2 density in the plasma at 20 mbar, while it is only higher than O_2 in the first half of the plasma at 100 mbar and between $z = 10$ cm and $z = 11$ cm at 1 bar.

Comparing the results given by the model using the full set and the reduced set, we can see that the agreement in the predicted density profiles is very good at 100 mbar and at 1 bar. At 20mbar, the agreement is also reasonably good at the end of the plasma and in the afterglow, but the model with the reduced set somewhat overestimates the O_2 density and underestimates the O density in the plasma itself. However, these densities are several orders of magnitude lower than the CO_2 density, and this deviation does not really affect the CO_2 conversion, which is the most important outcome of the model.

At 100 mbar, a small underestimation of the O density using the reduced set is found in the afterglow. This can be explained by the fact that the vibrational levels of O_2 are not included at this pressure, leading to a lower dissociation rate of O_2. As this

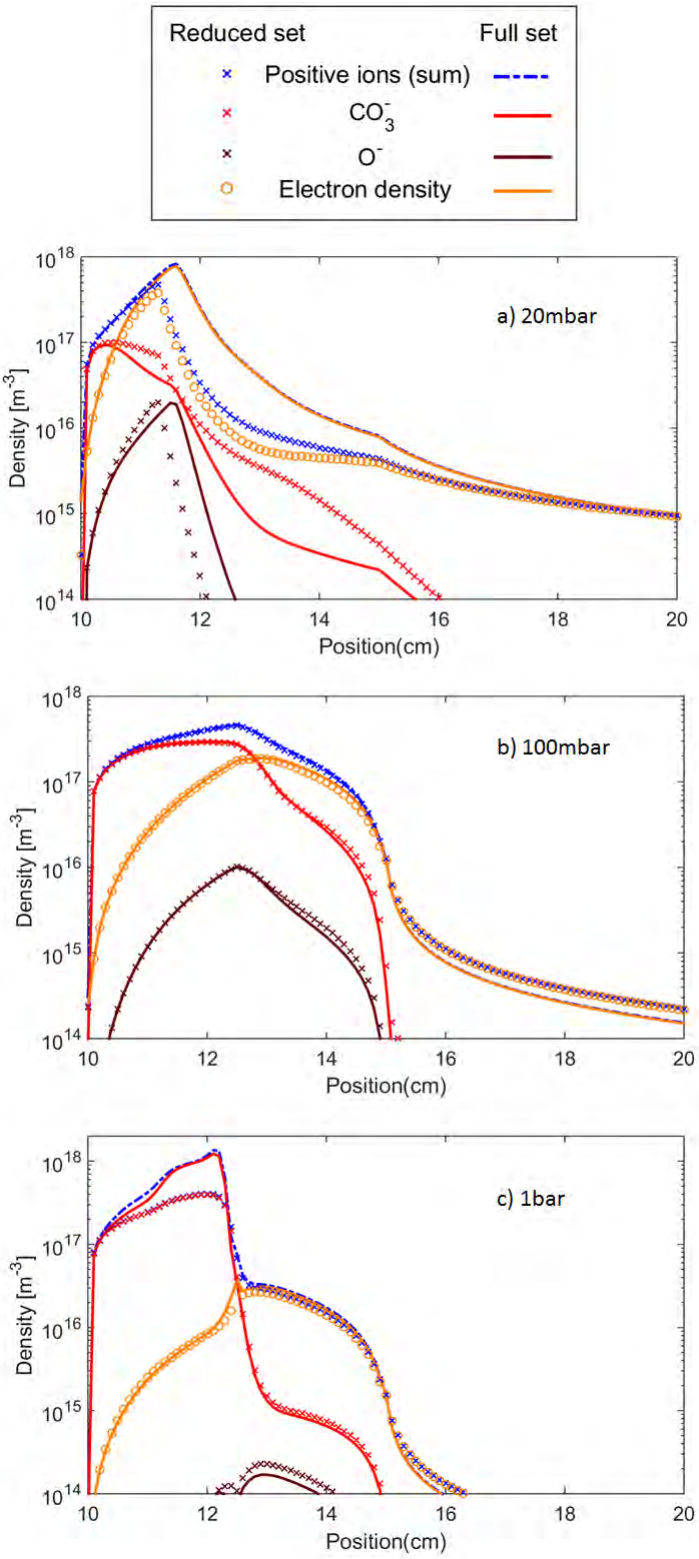

Figure 3. Comparison of the axial density profiles of the main charged species predicted by the full set (lines) and the reduced set (symbols) at p=20 mbar, 100mbar and 1bar and a SEI of 2.3 eV/molec

has no major influence on the CO_2 conversion, it was decided to leave these levels out at this pressure, to reduce the chemistry set as much as possible, in order to enhance its compatibility with more-dimensional models.

From these results, we can conclude that this first chemistry reduction has very little effect on the model predictions, certainly at 100mbar and above, at the conditions studied in this work.

3.2. Influence of the lumped-level strategy on the VDF and CO_2 conversion at fixed gas temperature

As previously mentioned, the results shown in this part are obtained using the temperature profile described in figure 1 and the reduced chemistry set. The model describing each vibrational level separately will be referred to as the "individual-levels" model. The predictions of the 3 different lumped models listed in table 3 as well as the model assuming a thermal vibrational distribution, called the "thermal distribution model", are compared to those of the individual-levels model. The accuracy of the level lumping method is tested in the entire pressure range between 20 mbar and 1 bar.

Figure 5 (left panel) shows the VDFs obtained by the different models at the beginning of the plasma (z=10.2cm), where the gas temperature is low (around 500K) and there is strong non-equilibrium, for pressures of 20mbar (a), 100mbar (b) and 1bar (c). The shape of the VDF predicted by the individual-levels model is very similar to our previous results obtained with the full chemistry set [9, 10] .

In a Maxwellian energy distribution, the vibrational temperature is given by the slope of the VDF (on a logarithmic scale). When the VDF becomes more complex (i.e., not a straight line on a logarithmic scale), it is still possible to define several vibrational temperatures using the different slopes, which correspond to different groups within the vibrational level population. We can clearly identify three groups in the VDF calculated by the individual-levels model at the three pressures shown here. The first vibrational levels [v_1 - v_3] appear to be in close-to thermal equilibrium, with a vibrational temperature of about 580K and 510K, at 100mbar and 1bar, respectively. At 20 mbar, the vibrational temperature of the first levels is slightly higher, reaching about 840K. A second part of the VDF [v_4 - v_{17}] is in non-equilibrium with vibrational temperatures several times higher than the gas temperature, i.e. from 5900K to 6200K. Finally, the last few levels [v_{18} - v_{21}] are overpopulated compared to a thermal VDF but the slope indicates that the vibrational temperature is here again close to the gas translational temperature, i.e. about 470K when considering the last two levels. This typical shape in 3 parts with different vibrational temperatures in the plasma motivates our choice of a 3-groups model, described by 3 different temperatures.

To understand the advantage of such a model, we compare it with two other lumped models, using 1 and 2 groups (see table 3), as well as a model yielding a thermal distribution. It should be noted that each extra group adds two extra equations to solve: one for the total number density of that group and one for the mean vibrational

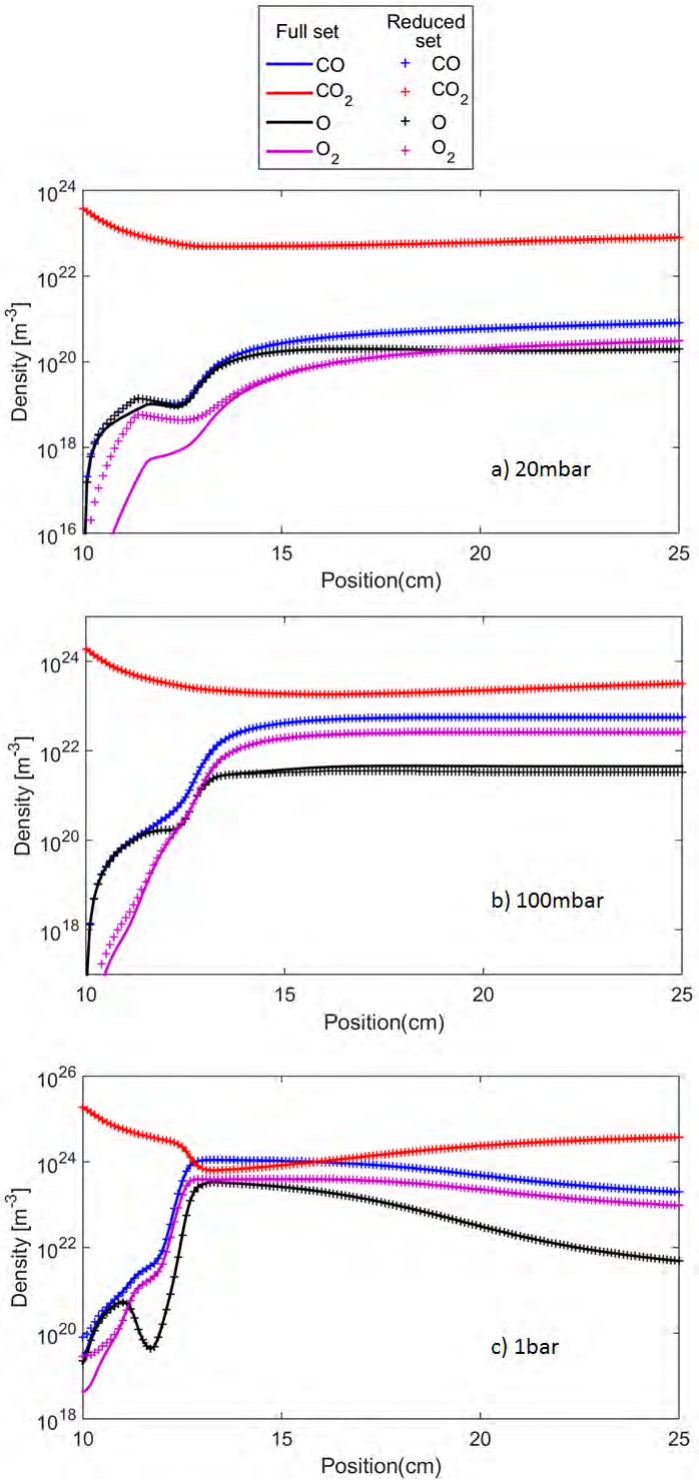

Figure 4. Comparison of the axial density profiles of the most important species predicted by the full set (lines) and the reduced set (crosses) at p=20 mbar, 100mbar and 1bar and a SEI of 2.3 eV/molec

energy of that group, representing the inner-distribution of the levels within each group. Therefore, there is a balance between accuracy of the model predictions and computational cost. This is the reason why we have not tested models with 4 or more groups, as their advantage in terms of computational cost compared to the individual-levels model would be limited.

It is clear from the left panel of figure 5 that the VDFs predicted by the 1-group model and the thermal distribution fail to reproduce the typical shape of the VDF in the beginning of the plasma and they result in a strong under-estimation of the population of the higher vibrational levels [v_5 - v_{21}]. The 2-groups model is able to reproduce the slope in the middle part of the VDF and thus it can be considered in reasonable agreement with the individual-levels model. However, the levels [v_{18} - v_{21}] are overestimated, as the last part of the VDF is not described by an extra group.

Finally, the VDF predicted by the 3-groups model yields quite good agreement with the individual-levels model, as it can reproduce the 3 parts of the VDF described above. A small deviation in the population of the highly excited vibrational levels is, however, still observed.

The right panel of figure 5 shows the VDFs obtained at the end of the plasma (i.e. z=14cm), where the gas temperature is about 2900K (see figure 1 above) at the same pressures. The individual-levels model predicts that the levels [v_1 - v_{14}] can be described with one slope only, with a vibrational temperature close to the gas temperature. The levels [v_{15} - v_{21}] are underpopulated compared to a thermal distribution, which can be explained by the high dissociation rate of the highly excited vibrational CO_2 levels. Indeed, the CO_2 dissociation in a MW plasma mainly proceeds by vibrational excitation to the lower levels, followed by VV relaxation, gradually populating the higher vibrational levels (so-called vibrational pumping or ladder climbing), and the latter will be subject to the dissociation[26].

Looking at the definition of the groups in Table 3 above, it is clear that the (one) group of the 1-group model, as well as both groups of the 2-groups model and the first two groups of the 3-groups model, adopt a vibrational temperature close to the gas temperature. Therefore, all the group models (1, 2 and 3-groups) manage to accurately reproduce the first thermal part of the VDF. The same applies to the model with the thermal distribution, which is quite logical. However, only the 3-groups model is able to reproduce rather accurately the last part of the VDF, as it considers a separate group for these last levels.

Note that it looks like the VDFs predicted by the 2-groups model and the 3-groups model exhibit only 1 and 2 slopes, respectively, but that is because both groups in the 2-groups model and the first two groups in the 3-groups model yield the same vibrational temperature, so their slopes coincide.

To evaluate whether the VDFs can be reproduced by the well-known Treanor distribution [27], we compare in Figure 6 the VDFs calculated by the individual levels model in the beginning of the plasma (i.e. z=10.2cm) and several Treanor distributions, using the gas temperature T_g=500K and several vibrational temperatures, as indicated

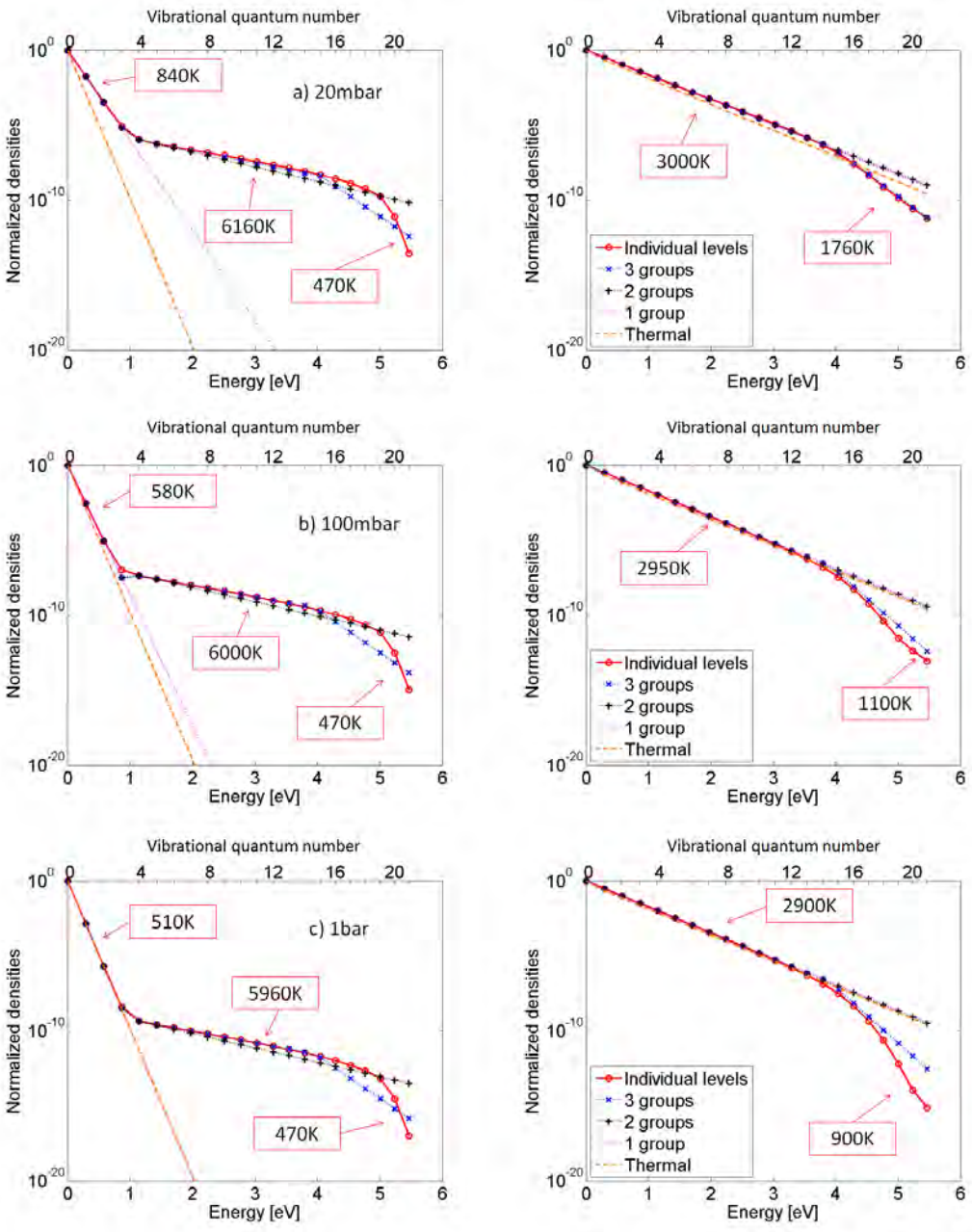

Figure 5. Non-equilibrium VDF in the beginning of the plasma (left) at z=10.2cm, and close-to-equilibrium VDF at the end of the plasma (right) at z=14cm, at 3 different pressures and a SEI of 2.3eV/molec. The vibrational temperatures corresponding to the different slopes of the VDF calculated with the individual-levels model are indicated. Comparison is made with the VDFs predicted by the different group models and the thermal distribution model.

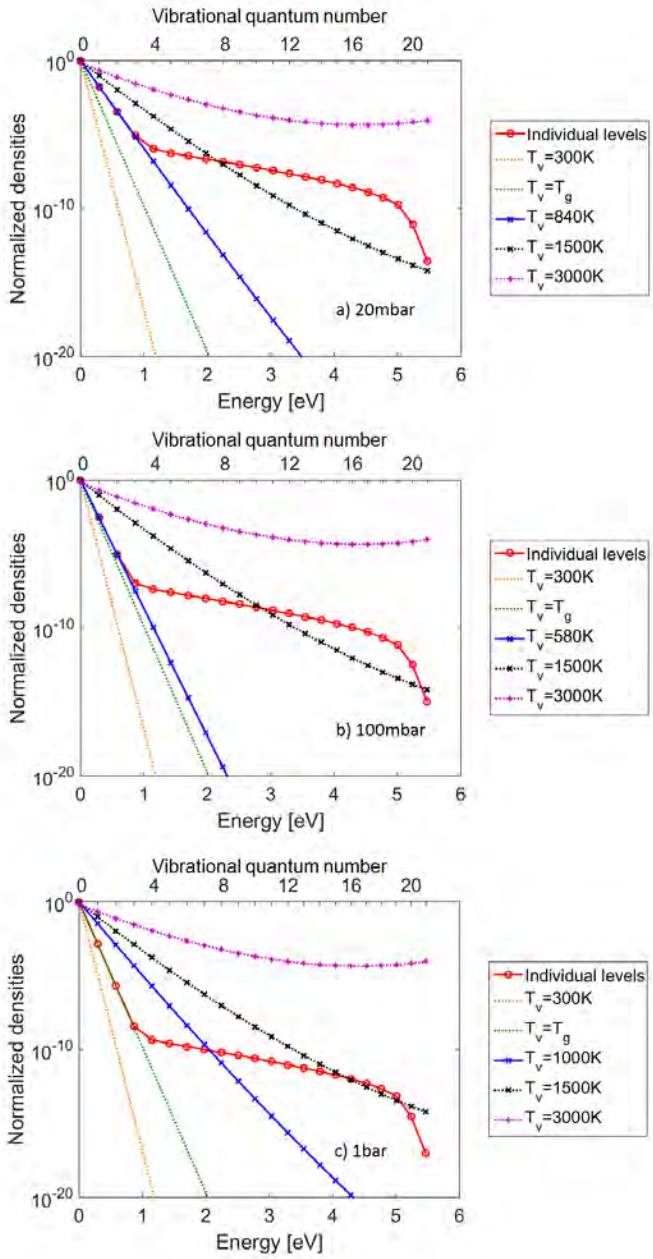

Figure 6. Non-equilibrium VDF in the beginning of the plasma at z=10.2cm at 3 different pressures and a SEI of 2.3eV/molec. Comparison is made between the VDF predicted by the individual level model and several Treanor distributions using different vibrational temperatures.

Table 5. Comparison of the CO_2 conversion predicted by the individual-levels model and the different lumped-levels models and the thermal distribution model at five different pressures and a SEI of 2.3eV/molec, using the temperature profile of figure 1. The relative errors given by the various lumped-levels models and the thermal distribution model are indicated between brackets, in %

	CO_2 conversion (%) and [Relative difference]				
Pressure	Individual-levels	3-groups	2-groups	1-group	Thermal
20 mbar	1.15	1.14 [-0.7%]	1.56 [+36%]	1.34 [+17%]	0.95 [-17%]
100 mbar	15.2	15.7 [+3%]	18.1 [+19%]	18.0 [+19%]	16.6 [+9%]
200 mbar	25.1	25.3 [+0.8%]	26.4 [+5.3%]	27.0 [+7.5%]	25.9 [+3.1%]
500 mbar	10.8	10.8 [+0.3%]	10.9 [+1.2%]	11.0 [+1.5%]	10.9 [+0.5%]
1 bar	4.57	4.58 [+0.2%]	4.63 [+1%]	4.76 [+4%]	4.58 [+0.2%]

in the legend. It is clear that the Treanor distributions all fail to reproduce the VDFs predicted by the model for any vibrational temperature and at any pressure. Indeed, only a vibrational temperature equal to the vibrational temperature of the first group can give a distribution reproducing accurately the first part of the VDF. However, the tail of the VDF is then overestimated. On the other hand, a larger vibrational temperature gives an overestimation of the first levels and can, in the more extreme cases, give an overestimation of the whole VDF (except the ground level). From these results, it seems that the Treanor distribution is a too rough approximation of the shape of the VDF, which stresses the need of using several groups with different vibrational temperatures, to accurately describe the actual VDF.

Table 5 shows the calculated CO_2 conversion of the different models at 5 different pressures (20, 100, 200 and 500 mbar, and 1 bar). The values given by the individual-levels model are in good agreement with the values given above, in table 4. The small differences can be explained by the use of two different codes (i.e., ZDPlaskin for the chemistry reduction and Comsol Multiphysics for the level-lumping method) and the fact that the first code self-consistently solves the EEDF, while the second code uses an external Boltzmann solver, as explained in section 2.4 above. As discussed in [12, 28, 29], in some cases, the effect of the EEDF on the CO_2 dissociation can be rather large and an a-priori calculation of the rate coefficients using an external Boltzmann solver can be a strong approximation when the EEDF greatly differs from a Maxwellian EEDF.

In all the cases tested here, the CO_2 conversion calculated with the 3-groups model is in reasonable agreement with the results of the individual-levels model. The 1 and 2-groups models and the model assuming a thermal distribution are not in good agreement with the individual-levels model for the pressures of 20 and 100 mbar. At 200 and 500 mbar, the agreement gradually becomes better, and at 1 bar, all the models are in quite good agreement with the individual-levels model. Indeed, at this pressure, the plasma is more or less thermal, and the CO_2 conversion mainly takes place at the end of the plasma, where the VDF approaches a simple Maxwellian distribution based on the gas temperature, at least up to level v_{14} (see right panel of figure 4(c)).

In the different models presented in this paper, most of the CO_2 conversion is attributed to reactions N1, N2 and N5 (see table A4). For pressures up to 200mbar, these reactions mainly occur from the highly excited vibrational levels, which are easily populated by electron impact excitation and VV transfer. However, for the higher pressures, the electron temperature is slightly lower, and the electrons mainly populate the lowest vibrational levels, at least in the region where most CO_2 conversion takes place (i.e., at the end of the plasma; cf. the right panel of figure 5c). Thus, for pressures above 200 mbar, the above-mentioned heavy-particle reactions mainly responsible for CO_2 dissociation, mostly occur from the CO_2 ground state, the symmetric mode vibrational levels and the first few asymmetric mode vibrational levels. Therefore, although only the 3-groups model is able to reproduce the VDF obtained by the individual-levels model, including the tail, it appears that at these conditions, the VDFs predicted by the other lumped-levels models , as well as by the thermal distribution model, are close enough to the real VDF to obtain a reasonable value for the CO_2 conversion, because the tail of the VDF plays a minor role.

It should be noted that the 2-groups model appears to give the worst agreement in CO_2 conversion at the lowest pressures, despite the fact that it better reproduces the VDF in the beginning of the plasma (cf. figure 5; left panel) compared to the 1-group models and the model assuming a thermal distribution. This may seem counter-intuitive. However, it can be explained as follows. At all the conditions investigated, the 2-groups model tends to systematically over-estimate the VDF at the higher vibrational levels (see e.g. figure 5 above). This results in an overestimation of the CO_2 conversion, because of the major role of the highest CO_2 vibrational levels in the CO_2 dissociation at low pressure (cf. above). On the other hand, the 1-group model and the model assuming a thermal distribution underestimate the VDF in the non-equilibrium part and overestimate it in the thermal part of the discharge (see figure 5: left and right panel, respectively). These two effects tend to compensate each other for predicting the overall CO_2 conversion, but the agreement can therefore not be considered better than with the 2-groups model.

For the same reason, the thermal model appears to give somewhat better results than the 1-group model: while the differences in the predicted VDFs are barely visible on the log-scale in figure 5, the vibrational temperature predicted by the 1-group model is systematically higher than the gas temperature. Therefore, the 1-group model predicts asymmetric mode vibrational levels populations that are slightly higher than the thermal model, explaining why the thermal model predicts a conversion slightly lower than the 1-group model. Again, the agreement given by the thermal model can therefore not be considered better than with the 1-group model.

3.3. Influence of the lumped-level strategy on the various plasma characteristics and CO_2 conversion in a self-consistent calculation

In this section, we assess the validity of the lumped-levels models, by comparing the calculated gas temperature, electron density, electron temperature and VDF in the plasma, as well as the obtained CO_2 conversion, with the results of the individual-levels model. Furthermore, we also compare to the model assuming a thermal distribution and a model not considering the asymmetric mode vibrational excitation (i.e. the CO_2v_i levels) at all. For this assessment, we self-consistently calculate the gas translational temperature T_g using equation 6.

3.3.1. Effect on the gas temperature profile Figure 7 (left panels) shows the axial profile of the gas temperature, calculated by the different models, at pressures of 20 mbar, 100 mbar and 1 bar. At 20 mbar and 100 mbar, the individual-levels model predicts a peak in the gas temperature profile of T_g=3280K and T_g=2920K at about z=14.5cm and z=13.5cm, respectively. The fact that the gas temperature is slightly lower at higher pressure is counter-intuitive, but can be explained from the relative importance of various (exothermic and endothermic) heavy particle reactions, as outlined below. Subsequently, the gas temperature starts to drop slowly, indicating that part of the translational energy goes to the vibrationally excited levels. At 1 bar, the gas temperature increases from the beginning of the plasma to approximately z=13cm and then forms a plateau at T_g=2420K. This shape, as well as the lower gas temperature at this higher pressure, can be explained as follows.

Figure 7 (right panels) shows the heat released (positive value) or absorbed (negative value) by the different reactions, as calculated by the individual level model, at pressures of 20 mbar, 100 mbar and 1 bar.

In each case, VT relaxation is the main source of translation energy for the heavy particles, and thus the main reason for gas heating. At 20 and 100 mbar, our calculations reveal that this is the case from the beginning of the plasma to z=14cm. At this stage, the dissociation of CO_2 by heavy particle impact (Reaction N1 in table A4) starts playing a more important role and explains why the gas temperature drops, as this reaction is endothermic. On the other hand, at 1bar, VT relaxation is only the major source of translational energy for the heavy particles (and thus of gas heating) until z=13cm. At this position, reaction N1 starts counterbalancing the effect of VT relaxation, explaining why the temperature stops increasing. However, from z=13.5cm, the exothermic recombination reactions (N3, N4 and N9 in table A4) become non-negligible. The VT energy exchanges eventually give a negative contribution to the gas heating, as the tail of the VDF is underpopulated. Thus, the VT relaxation and the various heavy particle endothermic and exothermic reactions balance each other and the variation of gas temperature becomes very small. This explains why the gas temperature at p=1bar becomes constant from z=13cm to the end of the simulation region.

The 1-, 2- and 3-groups models almost perfectly manage to reproduce this behavior,

although a slight deviation is seen for the 1- and 2-groups models at 20 mbar.

The model without vibrational excitation (see green curve in figure 7) shows a slower rise of temperature, followed by a plateau at T_g=1280K, T_g=1780K and T_g=1930K, for p=20mbar, p=100mbar and p=1bar, respectively, indicating that the gas temperature stays constant in the post-plasma region. Since the asymmetric mode vibrational excitation is not taken into account in this model, the main source for the gas temperature is VT relaxation from the 4 symmetric mode levels taken into account. Moreover, the reactions mentioned before (i.e. N1, N3, N4 and N9 in table A4), have a negligible contribution to the gas temperature in this case. Indeed, N1 can only occur from the ground state of CO_2 in this model, and thus it is of minor importance because of the high activation energy of this reaction (see exponential term in the rate coefficient). Furthermore, as the CO_2 dissociation is not very efficient without asymmetric mode vibrational excitation, yielding only a minor CO_2 conversion of less than 2% (see table 6 below), the CO and O_2 densities remain small in the whole simulation domain, and the exothermic reactions N3, N4 and N9 play a negligible role.

A similar trend is predicted by the model assuming a thermal distribution, but the plateau is at a much lower temperature of T_g=590K and T_g=640K, for p=20mbar and p=100mbar, respectively. At p=1bar, this model predicts a maximum gas temperature of only 560K, followed by a slow drop. The fact that this model cannot reproduce the gas temperature calculated by the individual-levels model can be explained by the influence of VT energy exchanges on the calculation of the gas temperature. Indeed, the 1-, 2- and 3-group(s) models solve for the density of the vibrational levels as well as the mean energy contained in the asymmetric mode vibrational excitation (i.e., by solving the equations for the total density and the mean energy of each group, which gives the slope of the VDF and thus the inner-distribution). Therefore, they guarantee that the total energy is conserved and they are able to accurately reproduce the gas temperature. The thermal distribution model, however, simply assumes that the population of the asymmetric mode vibrational levels is in thermal equilibrium with the gas temperature. As seen in figure 5 above, this assumption is generally not valid for a CO_2 microwave plasma at the conditions investigated. The loss terms for the gas temperature and electron energy due to the energy transfer towards the vibrational levels are still present but they do not give rise to a larger vibrational energy. Therefore, the thermal distribution model does not guarantee conservation of energy, which results here in a loss of energy, explaining the lower gas temperature.

The model not considering the vibrational excitation obviously also does not account for the VT relaxation, and thus, this leads here to a lower gas temperature. On the other hand, it still guarantees energy conservation, so the gas temperature is still in somewhat better agreement with the individual-levels model, compared to the thermal distribution model.

These results show the importance of a correct description of the vibrational energy in a self-consistent model. Thus, we may conclude that the thermal distribution model and the model not taking asymmetric mode vibrational excitation into account cannot

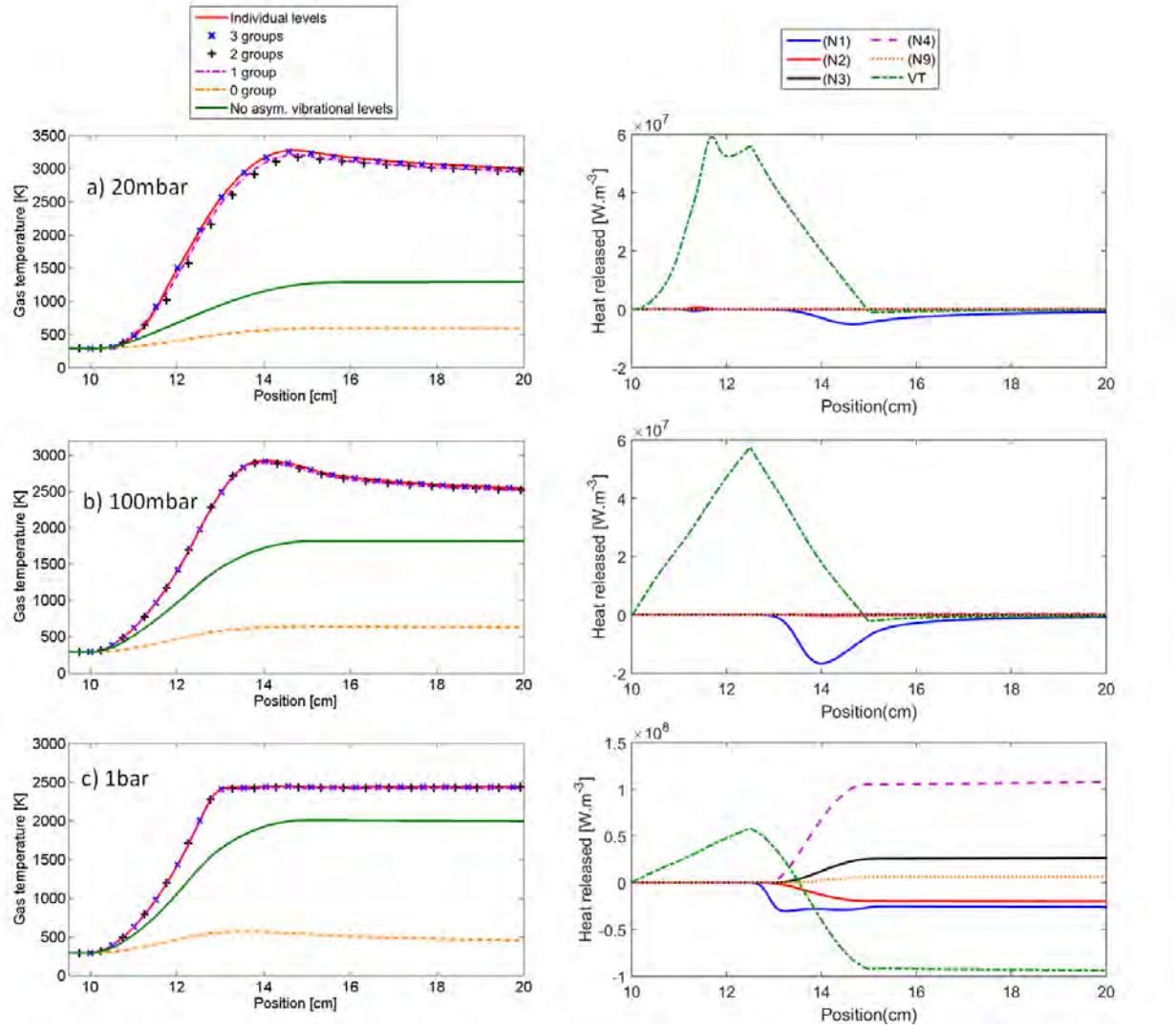

Figure 7. Left panels: Axial profile of gas temperature, calculated by the different models (see legend) at three different pressures and a SEI of 2.3 eV/molec. Right panels: Heat released or absorbed by the most important reactions, calculated by the individual levels model.

predict the correct gas temperature in a MW plasma. The 1-, 2- and 3-group(s) models, on the other hand, can well reproduce the gas temperature calculated by the individual-levels model. Nevertheless, it should be kept in mind that the CO_2 conversion is not well reproduced by the 1- and 2- group(s) models (see section 3.2 and also below).

3.3.2. Effect on the electron density Figure 8 (left panels) shows the axial profiles of electron density for a pressure of 20mbar, 100mbar and 1bar. The same behavior was also observed at the other pressures investigated. The electron density calculated by the individual-levels model shows a quasi-triangular profile with maxima of $7.10^{17}m^{-3}$, $1.7.10^{17}m^{-3}$, and $2.5.10^{16}m^{-3}$, at 20mbar, 100mbar and 1bar, respectively. A drop in

electron density at rising pressure seems counter-intuitive, but can be explained because the length of the plasma (L in figure 1) and the power deposition were kept constant in all the simulations. Thus, at constant power density, the electron temperature will be somewhat higher at lower pressure (see below), as the electrons lose less energy by collisions with the gas molecules. This higher electron temperature gives rise to more electron impact ionization, explaining the higher electron density at lower pressure. In reality, we might expect that the plasma length will decrease with rising pressure, so the power would be focused in a smaller volume at higher pressure, giving rise to a higher electron density. Radial contraction of the plasma at high pressure is also expected. However, this behavior is difficult to reproduce with a 0D model. Note, however, that the different electron attachment reactions also play a larger role at atmospheric pressure, reducing the electron density.

The fact that the electron density profile at 1 bar does not follow exactly the power-deposition profile, but keeps on rising until about z=13.3 cm, is due to the presence of O_2^- and CO_3^- ions in relatively large amounts in the plasma. They keep on providing electrons, mostly through reaction (I10) followed by reaction (I9) (see table A2).

This quasi-triangular profile is well-reproduced by the 1-, 2- and 3-group(s) models, both in shape and absolute value. On the other hand, the thermal distribution model and the model without asymmetric mode vibrational excitation are able to reproduce the shape of the electron density, which is mostly determined by the shape of the deposited power (see figure 1 above), but they predict clearly different values. Furthermore, at 1bar, the maxima of electron density predicted by the thermal distribution model and the model without asymmetric mode vibrational excitation are shifted to the center of the plasma.

The electron density calculated by the thermal distribution model is a factor 3 - 4 too low at all pressures investigated, while the model without asymmetric mode vibrational excitation predicts an electron density which is approximately a factor 2, 3 and 4 too high, at 20mbar, 100mbar and 1bar, respectively. As discussed above, the thermal distribution model does not guarantee conservation of energy, resulting in a loss of the total energy. Less energy is then available for the different ionization reactions, resulting in a lower electron density. On the other hand, the model which does not consider asymmetric mode vibrational excitation results in a somewhat larger electron energy density (or temperature; see below). Indeed, vibrational excitation is one of the main energy losses for the electrons due to its much lower energy threshold than electronic excitation and ionization processes. Since vibrational excitation to the asymmetric mode vibrational levels is not included in this model, this results in a somewhat larger electron energy density, thus yielding more electron impact ionization, and thus a larger electron density.

3.3.3. Effect on the electron temperature The effect on the electron temperature can be seen in the right panel of figure 8. The individual-levels model predicts an electron temperature of 0.8 eV in the beginning of the plasma (z=10cm) at all pressures

	CO_2 conversion (%) and [Relative difference]					
Pressure	Individual-levels	3-groups	2-groups	1-group	Thermal	No $CO_2 v_i$
20 mbar	14.4	9.99 [-30%]	23.4 [+63%]	13.8 [-4%]	0.1 [-99%]	1.55 [-89%]
100 mbar	16.5	16.5 [+0.3%]	17.9 [+8.5%]	16.8 [+2.3%]	0.07 [-99.6%]	1.5 [-91%]
200 mbar	15.7	15.9 [+0.3%]	17.0 [+8.5%]	16.1 [+2.3%]	0.06 [-99.6%]	1.1 [-93%]
500 mbar	17.6	17.5 [-0.5%]	18.4 [+4.6%]	18.9 [+7.3%]	0.06 [-99.7%]	1.0 [-94%]
1 bar	18.7	18.8 [+0.4%]	19.4 [+3.8%]	19.0 [+1.7%]	0.04 [-99.8%]	1.2 [-93%]

Table 6. Comparison of the CO_2 conversion predicted by the individual-levels model, the different lumped levels models, the thermal distribution model and the model without asymmetric mode vibrational excitation, at five different pressures and a SEI of 2.3eV/molec, using the self-consistent gas temperature calculation. The relative errors given by the lumped levels models, the thermal distribution model and the model without asymmetric mode vibrational excitation are indicated between brackets, in %

investigated. It increases to 0.9 eV at 100 mbar and to 1.2 eV at 20 mbar, at around z=13cm, followed by a weak drop till z=15 cm, which can be explained by the power deposition profile (see figure 1 above). At z=15cm, the power deposition stops, which results in a fast drop in the electron temperature. At p=1bar, the individual-levels model does not predict a rise in the electron temperature in the plasma, but values of T_e varying between 0.7 eV and 0.8 eV, followed again by a drop, which starts already at z>12.5cm. This is attributed to the fact that the electron density keeps on increasing even after the maximum power deposition density (i.e. at z=12.5cm) has been reached (see figure 8 (c), left panel), leaving less energy to more electrons and thus reducing the electron temperature.

Again, the 1-, 2- and 3-group(s) models are more or less able to reproduce these calculated electron temperature profiles, although at 100mbar and 1bar, the 2-groups model predicts a somewhat lower electron temperature between z=11cm and z=12cm. On the other hand, the thermal distribution model and the model without asymmetric mode vibrational excitation fail to accurately reproduce the shape and absolute value of the electron temperature profiles at the different pressures investigated. However, the differences are smaller than for the gas temperature or the electron density. Indeed, in a microwave plasma, for a given pressure, the electron temperature tends to show little variation upon different conditions, as observed in [30] and discussed more in detail in [20].

3.3.4. Effect on the CO_2 conversion Table 6 shows the CO_2 conversion predicted by the various models, as well as the relative differences with the individual-levels model. The results are clearly different from the comparison shown in table 5. The reason is that the CO_2 conversion largely depends on the gas temperature, and the self-consistently calculated profiles (illustrated in figure 7) differ to some extent from the temperature-profile shown in figure 1, used to calculated the CO_2 conversion of table 5. This strong temperature dependence of the CO_2 conversion stresses the importance of a correct temperature calculation in the model.

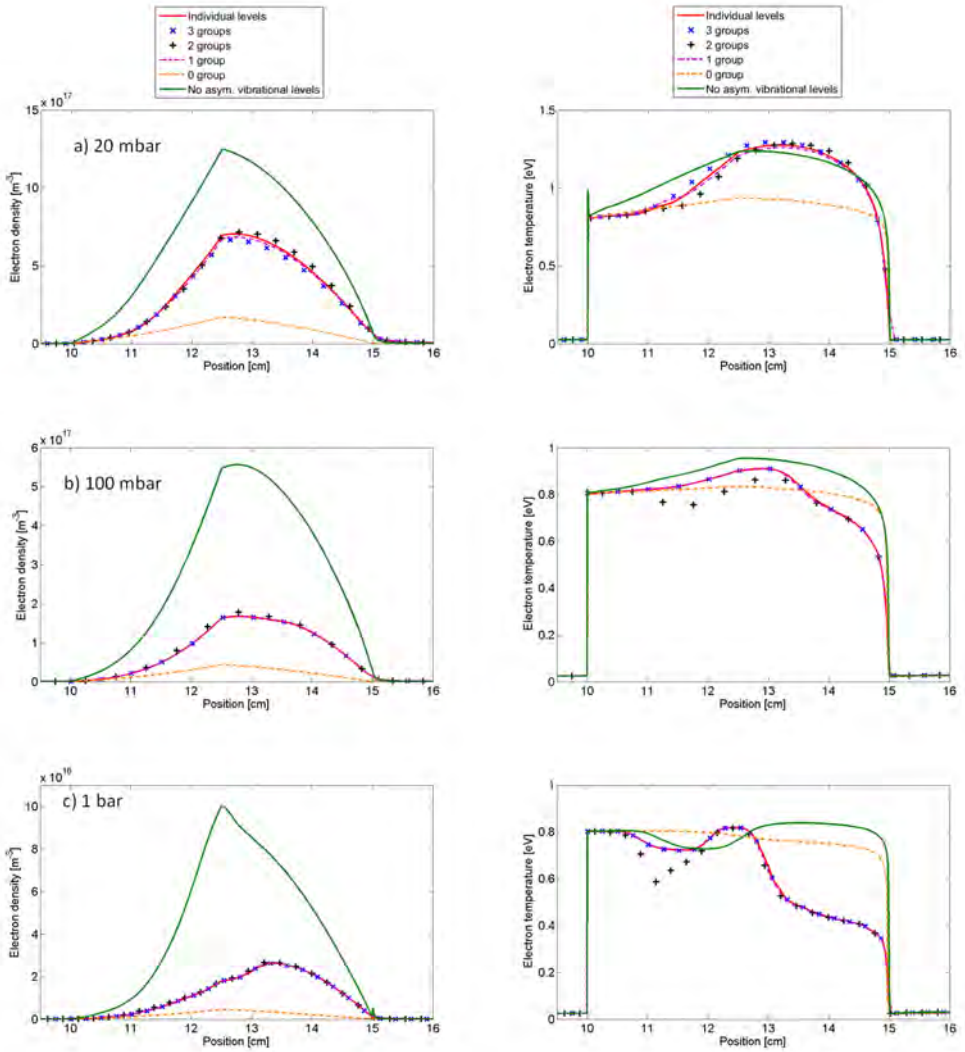

Figure 8. Axial profile of electron density (left) and temperature (right) inside the plasma, calculated by the different models (see legend) at three different pressures and a SEI of 2.3 eV/molec.

At 100 mbar, the CO_2 conversion predicted by both approaches is still in reasonable agreement, which is logical because the self-consistently calculated gas temperature profile (i.e., the second approach) is most similar to the profile assumed in the first approach (cf figure 1 and figure 7 b).

As is clear from table 6, at a pressure between 100mbar and 1bar, excellent agreement is observed for the CO_2 conversions calculated by the individual-levels model and the 3-groups models. The agreement is worse for the 2-groups model, but again slightly better for the 1-group model (except at 500mbar). This can again be explained by the fact that the 1-group model tends to underestimate the population of the highly excited levels in the non-thermal part of the plasma and to overestimate them in the

close-to-thermal-equilibrium part (see section 3.2 above and also next section), and these two effects compensate each other. The 2-groups model, on the other hand, tends to systematically over-estimate the population of the highly excited levels, resulting in a larger CO_2 conversion.

Due to the large differences in the calculated plasma characteristics (see previous sections) and the inaccurate or non-existent description of the vibrational energy contained in the asymmetric mode levels, the thermal distribution model and the model without asymmetric mode vibrational excitation are not able to reproduce the CO_2 conversion, predicted by the individual-levels model, at none of the pressures investigated. Indeed, the conversion predicted with these two models is far too low in each case, because they underestimate, or do not consider at all, the vibrational asymmetric mode levels. Furthermore, this also results in a lower gas temperature, as explained in section 3.3.1 above (see also figure 7 above). Therefore, they significantly underestimate both the conversion due to the ladder climbing effect mentioned above and the conversion due to purely thermal effects.

At 20mbar, even the 3- and 2-groups models are not in good agreement with the individual-levels model, yielding an underestimation of the CO_2 conversion by 30% for the 3-groups model and an overestimation by 63% for the 2-groups model. The 1-group model appears to show a better agreement, with a CO_2 conversion underestimated by only 4%. However, this is again the result of the two competing effects, as explained below, and therefore, it does not mean at all that this model is more realistic. The reason why the 3- and 2-groups models do not yield a good agreement in the predicted CO_2 conversion at 20 mbar, in spite of the good agreement in calculated gas temperature, electron density and temperature, is because of the strong influence of the levels [v_{18}-v_{21}] on the CO_2 dissociation at this low pressure, and can be fully understood by looking at the VDFs calculated with the various models, as illustrated in the next section.

3.3.5. Effect on the VDFs The left panel of figure 9 shows the VDFs calculated by the different models in the plasma, at the axial position where the local CO_2 conversion reaches its maximum (i.e. z=11.5cm) at a pressure of 20mbar. The VDFs calculated at 100mbar and 1bar will be presented below, but we first focus on the VDF at 20mbar, to explain the discrepancy in the CO_2 conversion at this pressure.

The 3-groups model shows a somewhat better overall agreement with the individual-levels model than the 1- and 2-groups models. However, all the lumped-levels models underestimate the tail of the VDF, except for level v_{21}, which is overestimated by these models. The individual-levels model predicts that at this low pressure the dissociation of CO_2 from levels v_{18}, v_{19} and v_{20} directly contributes for more than 90% to the CO_2 dissociation at z=11.5cm. As these levels are underestimated by the 3-groups model, this explains the underestimation in the CO_2 conversion. The same effect also applies to the 1- and 2-groups models, but on the other hand, these models predict that the CO_2 dissociation from level v_{21} accounts for more than 90% of the total dissociation, since this level is overestimated by several orders of magnitude in these models. Moreover,

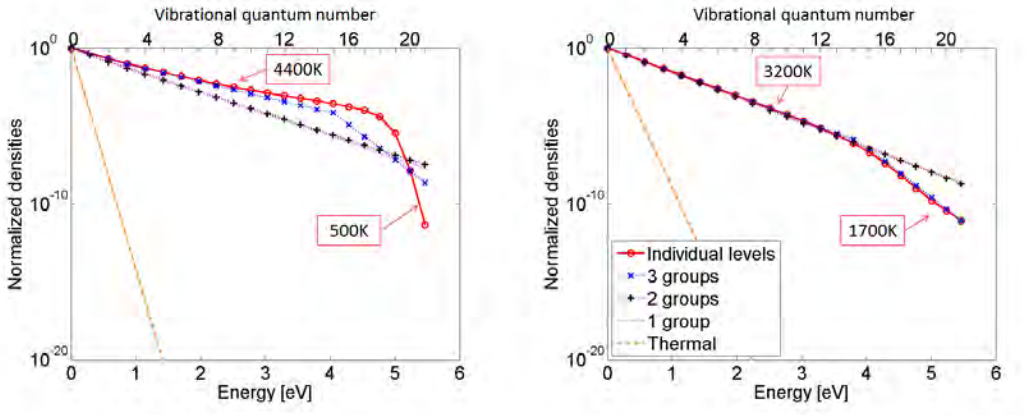

Figure 9. Non-equilibrium VDF at the position in the plasma with local maximum CO_2 conversion, i.e. at z=11.5cm (left), and close-to-equilibrium VDF at the end of the plasma at z=14cm (right), for a pressure of 20mbar and a SEI of 2.3eV/molec. The vibrational temperatures corresponding to the different slopes of the VDF calculated with the individual-levels model are also indicated. Comparison is made with the VDFs predicted by the different lumped-levels models and the thermal distribution model.

although it is barely visible on a logarithmic scale, the density of the $CO_2[v_{21}]$ level is 1.6 times higher in the 2-groups model than in the 1-group model at this position, resulting in a larger overestimation of the CO_2 dissociation. In the 1-group model, the overestimation of the dissociation from level v_{21} coincidently compensates for the underestimation of the dissociation from levels v_{18}, v_{19} and v_{20}. In the 2-groups model, as the overestimation of the dissociation from v_{21} is stronger, it gives rise to a larger CO_2 dissociation. Therefore, the better agreement with the 1-group model is the result of two competing effects and it should be considered with caution, as it might not be so good at other conditions.

The right panel of figure 9 illustrates the VDF at the end of the plasma (z=14 cm), calculated by the different models. It is clear that the 3-groups model almost perfectly reproduces the VDF of the individual-levels model, while the 1-group and 2-groups models strongly overestimates the higher vibrational levels ($> v_{15}$) and the thermal distribution model strongly underestimates all levels.

To explain the better agreement in the CO_2 conversion calculated by the 3-groups model and the individual-levels model at the higher pressures, we illustrate in figure 10 the VDFs at 100mbar and at 1 bar, at an axial position of z=10.2cm, where the VDF is in strong non-equilibrium (left panels), and at an axial position of z=14cm, where most of the CO_2 conversion takes place at these conditions (right panels). As we have seen above in figure 5, the VDF in the beginning of the plasma (left panels) is characterized by three different parts and the 3-groups model is the only model that can (more or less) reproduce this shape, although some underestimation of the tail of the VDFs is still visible.

Moreover, as is clear from the right panel of figure 10 at z=14cm, the 3-groups

model yields again the best agreement with the VDF predicted by the individual-levels model, although a small overestimation of the tail of the VDF is observed, especially at 1bar.

Most of the conversion appears at the end of the plasma (around z=14 cm) in this pressure range. As observed in section 3.2, most of the CO_2 dissociation originates from the ground state, the symmetric mode vibrational levels and the first asymmetric mode vibrational levels. This explains why all the lumped-levels are able to predict a correct CO_2 conversion, despite their overestimation of the tail of the VDF. However, as the tail of the VDF still plays a (minor) role, the 3-groups model still gives the most accurate values for the CO_2 conversion (except at 20mbar). It is interesting to note that because of the incorrect gas temperature calculated by the thermal distribution model, it is also not able to predict the shape of the VDF, even not the thermal parts. Therefore, when using a self-consistent gas temperature calculation, even in the case when CO_2 conversion also occurs in the close-to-thermal-equilibrium part of the discharge, the thermal distribution model cannot yield the right CO_2 conversion.

In certain conditions, especially at low pressure, the last levels of the VDF have a very strong influence on the CO_2 conversion as their vibrational energies are close to the dissociation energy. This shows that an accurate description of the tail of the VDF is crucial. In general, only the 3-groups model allows to (more or less) reproduce the tail of the VDF (except at the low pressure of 20mbar around z=11.5 cm; cf figure 9 left panel). Hence we believe it is the only model that can predict the correct CO_2 conversion. A better agreement reached by a lower-group model, that is not able to reproduce the VDF, can therefore only be the result of two competing effects. At the low pressure of 20mbar, in the middle of the plasma, even the 3-groups model seems to fail in reproducing the correct VDF, resulting in an underestimation of the CO_2 conversion.

3.4. Range of validity of the level-lumping method

From the results above, it is clear that the level-lumping method, especially with 3 groups, is able to reproduce the results of a model solving for each vibrational level separately, at the conditions studied in this paper. Only at 20mbar, the agreement is not satisfactory, but this pressure is not so much of interest for CO_2 conversion applications. It is also clear from above that conservation of energy is a crucial point.

Counting for the number of equations to solve, only taking into account the chemical kinetics part of the model, the full chemistry set from [9, 10] requires to solve 126 equations while the reduced chemistry set requires to solve for 36 equations (at a pressure of 100mbar and below), or 39 equations (at 200mbar and above). A further computational load reduction is achieved by lumping the levels. Indeed, in this case, the 21 equations representing the 21 individual vibrational levels can be removed, yielding only 15 (or 18) equations, plus 2 equations for each of the lumped levels. In this way, a n-groups model requires to solve for $15 + 2n$ equations (or $18 + 2n$ at 200mbar and

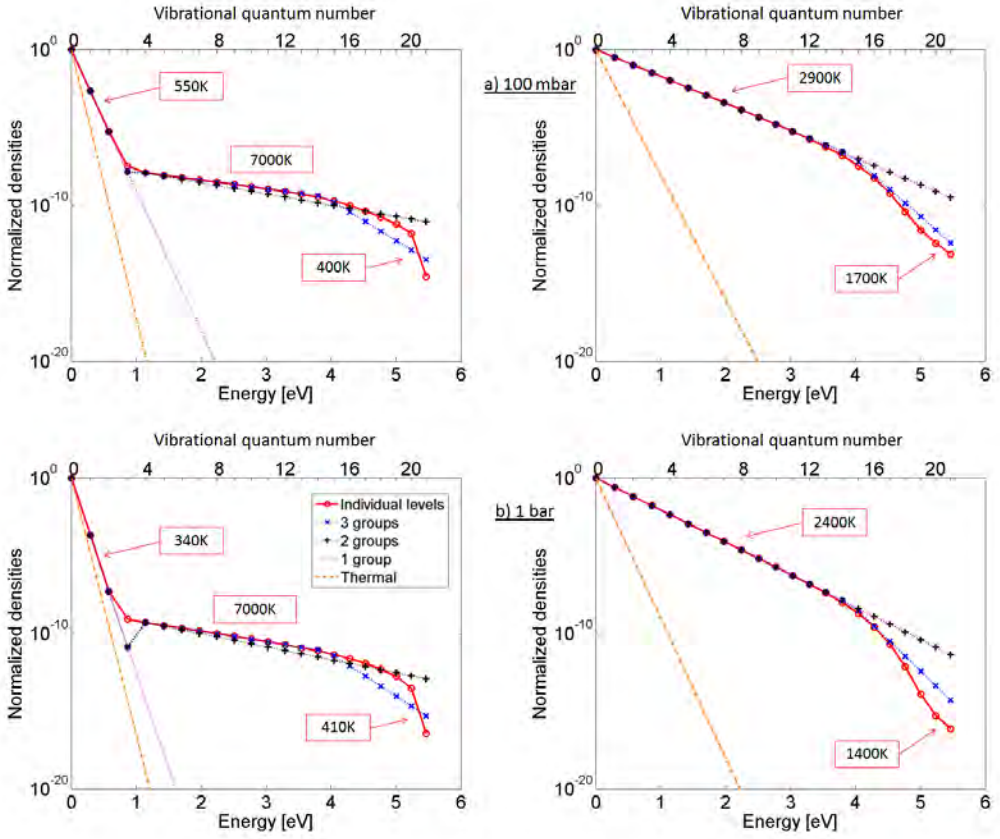

Figure 10. Non-equilibrium VDF in the beginning of the plasma (left) at z=10.2cm, and close-to-equilibrium VDF at the end of the plasma (right) at z=14cm, at 100mbar and 1bar and a SEI of 2.3eV/molec, computed using a self-consistent gas temperature calculation. The vibrational temperatures corresponding to the different slopes of the VDF calculated with the individual-levels model are also indicated. Comparison is made with the VDFs predicted by the different lumped-levels models and the thermal distribution model.

above) for the chemical kinetics part.

In our 0D-model, this computation time reduction caused by the level-lumping is not clearly visible, as the vibrational temperature can vary quite fast, counter-balancing the advantages of the reduction of the number of equations to solve. However, we expect the computational cost to significantly improve for a 1D, 2D or 3D model, as diffusion would smooth out the sharp peaks of the vibrational temperature seen in our 0D-model.

Despite the clear advantages of the level-lumping method, it should be stressed that it is not valid under all conditions that can exist in a CO_2 plasma.

Indeed, while studying the conditions presented above, we have also tested the validity of the method for more challenging conditions, to assess its range of applications. We noted that even the 3-groups model fails to accurately reproduce the VDF when the non-equilibrium part in the plasma is too strong, i.e. when the vibrational temperature is much larger than the gas-temperature. This effect was also apparent for the 20mbar case above. Moreover, using several groups, it can happen that, at the junction between

two groups, the model predicts $n_j < n_{j'}$ with $j < j'$, which is not a physical result. This is for example visible in figure 10 (b) (left panel) for levels V_3 and V_4.

By analysing the equations of the lumped-levels model, we see that the contribution of the energy of each level to the mean group energy $\overline{E_{g_i}}$, defined by equation 13, depends on its population. If we now look at the ratio of the contribution β of two levels j < j' within one group i, we get:

$$\beta = \frac{E_j n_j}{E_{j'} n_{j'}} \simeq \frac{E_j}{E_{j'}} exp(\frac{E_{j'} - E_j}{k_B T_{v_i}}) \tag{18}$$

β exponentially increases when $E_{j'}$ increases for a given j. This means that the contribution of the highly excited levels of one group to the mean vibrational energy of that group is small, under usual conditions of vibrational temperature ($k_B T_{v_i} < 1eV$). Changing the repartition of the levels between the different groups in a 3-groups model can help to describe more accurately the important parts of the VDF, as the population of the first levels of each group tends to be more accurately reproduced. Naturally, the optimal choice for this repartition (shown in table 3) is case-dependent. However, at the conditions under study, which are common for MW plasmas used for CO_2 conversion, the level-lumping method works quite well. More specifically, using a 3-groups model, it is possible to reproduce the shape of the VDF and the predictions of the individual-levels model reasonably well. Even the 2-groups model and the 1-group model predict results in reasonable agreement with the results of the individual-levels model, in spite of the fact that the VDF is not properly reproduced, as they are still able to predict the mean energy contained in the asymmetric mode vibrational levels. However, as shown above, an accurate description of the tail of the VDF is also important for a correct prediction of the CO_2 conversion. As the last levels of the VDF have small populations in comparison with the first levels, it is necessary to describe them using a separate group.

Finally, this (n-groups) level-lumping model only requires to solve n extra energy conservation equations, to determine the vibrational temperatures of the n groups, and n continuity equations for the corresponding number densities, which can be added to a standard plasma fluid model. It is thus very easy to implement in an existing code, which is one of its main advantages.

4. Conclusion

In this work, a reduced chemistry set to model CO_2 non-equilibrium discharges, with special focus on the CO_2 vibrational levels, is presented and compared to the complete chemistry set previously developed[9, 10]. Furthermore, a lumped-levels model is developed to avoid the need of solving equations for all individual CO_2 vibrational levels. The proposed chemistry reduction and level-lumping make this chemistry set compatible with the use in large-dimensional models (i.e. 1D, 2D and 3D) by drastically reducing the number of equations to solve, leading to a significant reduction of the calculation time.

We demonstrated that a 3-groups model is able to (more or less) reproduce the asymmetric mode vibrational distribution function of CO_2. Furthermore, this model also yields a good agreement with the full model for the different plasma quantities calculated (i.e., electron density and temperature, and gas temperature) as well as for the CO_2 conversion, in a range of different pressures, typically used in MW plasmas, i.e., between 100mbar and 1bar. However, both the reduction of the chemistry set and the level lumping are not entirely valid anymore at lower pressures (i.e. 20mbar). This should not be considered a big problem, as such low pressure is not really of interest for CO_2 conversion applications.

Also a 2-groups and 1-group model yield a very good agreement with the full model for the gas temperature and the electron density and temperature, and the agreement for the CO_2 conversion is still reasonable (at pressures of 200mbar and above), in spite of the fact that the VDF is not fully reproduced. At 1bar, these models also yield good agreement for the CO_2 conversion, because most of the conversion takes place in the part of the plasma where the VDF is in close-to-thermal equilibrium. There, the VDF resembles a simple Maxwellian distribution, except for the tail which appears to become less important at this high pressure. A further reduction of the number of equations to solve (i.e., by applying a thermal distribution model or a model without asymmetric mode vibrational excitation) leads to inaccurate results. This demonstrates the strong influence of vibrational excitation on the plasma characteristics. The balance between accuracy and computation time is here an important point.

Finally, our study reveals that the CO_2 conversion largely depends on the gas temperature. Indeed, the results obtained with the model assuming a fixed temperature profile are clearly different from the results obtained with the self-consistently calculated temperature. This indicates that the conversion, at these conditions, is partially due to thermal effects. A high gas temperature increases the population of all the vibrationally excited states, as well as the rate coefficients of the different (heavy particle) dissociation reactions. Both effects lead to a higher CO_2 conversion.

We also discussed the range of validity of the level-lumping method in CO_2 and we suggested possible ways to overcome the limitations. We believe that this level-lumping method can enable the modeling of CO_2 conversion in 2D or 3D microwave discharges, as it is quite easy to implement in an existing discharge code. This will be the subject of our future work.

5. Acknowledgement

This project has received funding from the European Union's Seventh Framework Programme for research, technological development and demonstration under grant agreement no 606889 and it was also carried out in the framework of the network on Physical Chemistry of Plasma-Surface Interactions—Interuniversity Attraction Poles, phase VII (PSI-IAP7) supported by the Belgian Science Policy Office (BELSPO). The computational work was carried out using the Turing HPC infrastructure at

the CalcUA core facility of the Universiteit Antwerpen (UA), a division of the Flemish Supercomputer Center VSC, funded by the Hercules Foundation, the Flemish Government (department EWI) and the UA.

Appendix A. List of chemical reactions

Table A1. Electron impact reactions. The rate coefficients are in $[m^3.s^{-1}]$ or $[m^6.s^{-1}]$ for two-body and three-body reactions, respectively, T_e in eV, T_g in K. EEDF means that the rate coefficients are calculated from the cross sections and the electron energy distribution function, calculated in Bolsig+ (see text in section 2.4 below).

No.	Reaction	Rate coefficient	Ref	Note
(X1)	$e+CO_2 \rightarrow e+CO_2$	EEDF	[31]	a
(X2)	$e+CO_2 \rightarrow 2e+CO_2^+$	EEDF	[31]	a
(X3)	$e+CO_2 \rightarrow O^-+CO$	EEDF	[31]	b
(X4)	$e+CO_2 \rightarrow e+O+CO$	EEDF	[31]	b
(X5)	$e+CO_2 \rightarrow e+CO_2^*$	EEDF	[32]	a
(X6a)	$e+CO_2 \rightarrow e+CO_2v_a$	EEDF	[23]	
(X6b)	$e+CO_2 \rightarrow e+CO_2v_b$	EEDF	[23]	
(X6c)	$e+CO_2 \rightarrow e+CO_2v_c$	EEDF	[23]	
(X6d)	$e+CO_2 \rightarrow e+CO_2v_d$	EEDF	[23]	
(X7)	$e+CO_2v_i \rightarrow e+CO_2v_j$	EEDF	[23]	c
(X8)	$e+CO \rightarrow e+CO$	EEDF	[23]	
(X9)	$e+CO \rightarrow C+O^-$	EEDF	[33]	
(X10)	$e+CO \rightarrow e+C+O$	EEDF	[34]	
(X11)	$e+O_2 \rightarrow e+O_2$	EEDF	[23]	
(X12)	$e+O_2 \rightarrow e+O+O$	EEDF	[23]	
(X13)	$e+O_2 \rightarrow O+O^-$	EEDF	[23]	
(X14)	$e+O_2 \rightarrow e+O_2v_i$	EEDF	[23]	i=1,2,3
(X15)	$e+O_2+M \rightarrow e+O_2^-+M$	EEDF	[23]	
(E1)	$e+CO_2^+ \rightarrow CO+O$	$2.0 \times 10^{-11}T_e^{-0.5}T_g^{-1}$	[35]	
(E2)	$e+CO_2^+ \rightarrow C+O_2$	$3.94 \times 10^{-13}T_e^{-0.4}$	[36]	
(E3)	$e+O+M \rightarrow O^-+M$	10^{-43}	[37]	

a) Same cross section also used for CO_2v_i (i = the various vibrationally excited levels)
b) Cross section also used for CO_2v_i, modified by lowering the energy threshold by the energy of the excited state of CO_2v_i
c) Cross section for the various levels (i,j) adopted from $e+CO_2v_0 \rightarrow e+CO_2v_1$, but scaled and shifted using Fridman's approximation [9, 2]

Table A2. Heavy particle reactions involving ions. The rate coefficients are in $[m^3.s^{-1}]$ or $[m^6.s^{-1}]$ for the two-body and three-body reactions, respectively.

No.	Reaction	Rate coefficient	Ref
(I1)[a]	$O^-+CO_2+M \rightarrow CO_3^-+M$	9.0×10^{-41}	[35]
(I2)	$O^-+CO \rightarrow CO_2+e$	5.5×10^{-16}	[36]
(I3)	$CO_3^-+CO \rightarrow 2CO_2+e$	5.0×10^{-19}	[35]
(I4)	$CO_3^-+CO_2^+ \rightarrow 2CO_2+O$	5.0×10^{-13}	[35]
(I5)	$O^-+O \rightarrow O_2+e$	2.3×10^{-16}	[38]
(I6)[a]	$O^-+M \rightarrow O+M+e$	4.0×10^{-18}	[39]
(I7)	$O_2^-+O \rightarrow O_2+O^-$	3.3×10^{-16}	[40]
(I8)	$O_2^-+O_2 \rightarrow O_2+O_2+e$	2.18×10^{-24}	[40]
(I9)[a]	$O_2^-+M \rightarrow O_2+M+e$	$2.7 \times 10^{-16}(\frac{T_g}{300})^{0.5}exp(-5590/T_g)$	[36]
(I10)	$O+CO_3^- \rightarrow CO_2+O_2^-$	8×10^{-17}	[35]
(I11)	$O_2^-+CO_2^+ \rightarrow CO+O_2+O$	6×10^{-13}	[35]

[a] M represents any neutral species taken into account in the model. The same rate coefficient is used for every species.

Table A3. Vibrational energy transfer reactions. The rate coefficients are in $[m^3.s^{-1}]$ and T_g is in K. The rates coefficients are given for the reaction between ground state and first vibrational level and are scaled for higher transitions.

No.	Reaction	Rate coefficient	Ref	Note
(V1)[a]	$CO_2v_x+M \leftrightarrow CO_2+M$	$7.14 \times 10^{-14}exp(-177T_g^{-1/3}+451T_g^{-2/3})$	[41]	$x=a,b,c,d$
(V2a)[a,b]	$CO_2v_1+M \leftrightarrow CO_2v_a+M$	$0.43 \times 10^{-6}exp(-407T_g^{-1/3}+824T_g^{-2/3})$	[41]	
(V2b)[a,b]	$CO_2v_1+M \leftrightarrow CO_2v_b+M$	$0.86 \times 10^{-6}exp(-404T_g^{-1/3}+1096T_g^{-2/3})$	[41]	
(V2c)[a,b]	$CO_2v_1+M \leftrightarrow CO_2v_c+M$	$1.43 \times 10^{-11}exp(-252T_g^{-1/3}+685T_g^{-2/3})$	[41]	
(V3)	$CO_2v_i+CO_2 \leftrightarrow CO_2v_{i-1}+CO_2v_x$	$2.13 \times 10^{-11}exp(-242T_g^{-1/3}+633T_g^{-2/3})$	[41]	$x=a,b$; $i \geq 2$
(V4)	$CO_2v_i+CO_2v_j \leftrightarrow CO_2v_{i-1}+CO_2v_{j+1}$	$1.8 \times 10^{-17}exp(24.7T_g^{-1/3}-65.7T_g^{-2/3})$	[42, 43]	$j \geq 1$
(V5)[a]	$O_2v_i+M \leftrightarrow O_2v_{i-1}+M$	$7.99 \times 10^{-11}exp(-320T_g^{-1/3}+615T_g^{-2/3})$	[41]	

[a] M represents any neutral species taken into account in the model. The same rate coefficient is used for every species.

[b] These reactions are also taken into account for v_i ($i > 1$), but then they are not considered separately, and the rate coefficient is then taken as the sum of V2a, V2b and V2c, leading to level CO_2v_{i-1}, because for the higher levels, no individual symmetric mode levels are included in the model. See [9] for more information

Table A4. Reactions of neutrals. Rate coefficients in $[m^3.s^{-1}]$ or in $[m^6.s^{-1}]$for the two-body and three-body reactions, respectively. T_g is in K. α is the parameter used to determine the rate constants of the same reactions with vibrationally excited CO_2 molecules. See [9] for more information

No.	Reaction	Rate coefficient	$\Delta H_r(eV)$	α	Ref
(N1)	CO_2+M → CO+O+M	$4.39 \times 10^{-13} exp(-65000/T_g)$	5.52	1.0	[2]
(N2)	CO_2+O → CO+O_2	$7.77 \times 10^{-18} exp(-16600/T_g)$	0.35	0.5	[2]
(N3)	CO+O+M → CO_2 + M	$8.2 \times 10^{-46} exp(-1510/T_g)$	-5.52		[37]
(N4)	O_2+CO → CO_2+O	$1.23 \times 10^{-18} exp(-12800/T_g)$	-0.35	0.5	[2]
(N5)	CO_2+C → CO+CO	1.0×10^{-21}	- 5.64		[39]
(N6)	O_2+C → CO+O	3.0×10^{-17}	-5.99		[37]
(N7)	CO+M → O+C+M	$1.52 \times 10^{-10} (T_g/298)^{-3.1} exp(-129000/T_g)$	11.16		[44]
(N8)	C+O+M → CO+M	$2.14 \times 10^{-41} (T_g/300)^{-3.08} exp(-2114/T_g)$	-11.16		[36]
(N9)	2O+M → O_2+M	$1.27 \times 10^{-44} (T_g/300)^{-1} exp(-170/T_g)$	-5.17		[45]

Appendix B. List of species removed from the full set

Table B1. Species described in full set that have been removed from the reduced set.

Neutral ground states
C_2O, O_3, C_2

Charged species
CO_4^+, CO^+, $C_2O_2^+$, $C_2O_3^+$, $C_2O_4^+$, C^+, C_2^+, O_2^+, O_4^+, O^+
CO_4^-, O_4^-, O_3^-

Excited states	State
$CO[v_{1-63}]$	
CO_2[e2]	$(^1\Delta_u)$
CO[e1]	$(A^3\Pi)$
CO[e2]	$(A^1\Pi)$
CO[e3]	$(A^3\Sigma)$ $(D^3\Delta)$ $(E^3\Sigma)$ $(B^3\Sigma)$
CO[e4]	$(C^1\Sigma)$ $(E^1\Pi)$ $(B^1\Sigma)$ $(I^1\Sigma)$ $(D^1\Delta)$
O_2[e1]	$(A^1\Delta)$ $(B^1\Sigma)$
O_2[e2]	$(B^3\Sigma)$ and higher triplet states

References

[1] "IPCC 2013, Fifth Assesment Report: Climate Change 2013 Synthesis Report ."

[2] A. Fridman, *Plasma chemistry*. New York: Cambridge University Press, 2008.

[3] R. I. Asisov, A. K. Vakar, V. K. Jivotov, M. F. Krotov, O. A. Zinoviev, B. V. Potapkin, A. A. Rusanov, V. D. Rusanov, and A. A. Fridman, "Non-equilibrium plasma-chemical process of CO_2 decomposition in a supersonic microwave discharge," *Proceedings of the USSR Academy of Sciences*, vol. 271, no. 1, 1983.

[4] L. F. Spencer and A. D. Gallimore, "Efficiency of CO_2 Dissociation in a Radio-Frequency Discharge," *Plasma Chemistry and Plasma Processing*, vol. 31, no. 1, pp. 79–89, 2011.

[5] L. F. Spencer and A. D. Gallimore, "CO_2 dissociation in an atmospheric pressure plasma/catalyst system: a study of efficiency," *Plasma Sources Science and Technology*, vol. 22, no. 1, p. 015019, 2013.

[6] T. Silva, N. Britun, T. Godfroid, and R. Snyders, "Optical characterization of a microwave pulsed discharge used for dissociation of CO_2," *Plasma Sources Science and Technology*, vol. 23, p. 025009, apr 2014.

[7] A. P. Goede, W. A. Bongers, M. G. Graswinckel, R. M. V. D. Sanden, L. Martina, K. Jochen, A. Schulz, and W. Mathias, "Production of Solar Fuels by CO_2 Plasmolysis," *3rd European Energy conference Budapest*, vol. 01005, pp. 1–5, 2014.

[8] W. A. Bongers, S. Welzel, D. C. M. V. D. Bekerom, G. Frissen, G. J. V. Rooij, A. P. H. Goede, M. F. Graswinckel, P. Groen, N. den Harder, B. van Heemert, T. Minea, M. van de Sanden, M. Leins, J. Kopecki, A. Schulz, and M. Walker, "Developments in CO_2 dissociation using non-equilibrium microwave plasma activation for solar fuels Energy Conversion," in *22nd International Symposium on Plasma Chemistry (Antwerp, Belgium)*, 2015.

[9] T. Kozák and A. Bogaerts, "Splitting of CO_2 by vibrational excitation in non-equilibrium plasmas: a reaction kinetics model," *Plasma Sources Science and Technology*, vol. 23, p. 045004, aug 2014.

[10] T. Kozák and A. Bogaerts, "Evaluation of the energy efficiency of CO_2 conversion in microwave discharges using a reaction kinetics model," *Plasma Sources Science and Technology*, vol. 24, no. 1, p. 015024, 2015.

[11] S. Heijkers, R. Snoeckx, T. Kozák, T. Silva, T. Godfroid, N. Britun, R. Snyders, and A. Bogaerts, "CO_2 Conversion in a Microwave Plasma Reactor in the Presence of N_2 : Elucidating the Role of Vibrational Levels," *The Journal of Physical Chemistry C*, vol. 119, no. 23, pp. 12815–12828, 2015.

[12] L. D. Pietanza, G. Colonna, G. D'Ammando, A. Laricchiuta, and M. Capitelli, "Vibrational excitation and dissociation mechanisms of CO_2 under non-equilibrium discharge and post-discharge conditions," *Plasma Sources Science and Technology*, vol. 24, no. 4, p. 042002, 2015.

[13] R. Aerts, T. Martens, and A. Bogaerts, "Influence of Vibrational States on CO_2 Splitting by Dielectric Barrier Discharges," *The Journal of physical chemistry C*, vol. 116, pp. 23257–23273, 2012.

[14] R. Aerts, W. Somers, and A. Bogaerts, "Carbon Dioxide Splitting in a Dielectric Barrier Discharge Plasma: A Combined Experimental and Computational Study," *ChemSusChem*, vol. 8, no. 4, pp. 702–716, 2015.

[15] K. Peerenboom, A. Parente, T. Kozák, A. Bogaerts, and G. Degrez, "Dimension reduction of non-equilibrium plasma kinetic models using principal component analysis," *Plasma Sources Science and Technology*, vol. 24, p. 025004, apr 2015.

[16] H. P. Le, A. R. Karagozian, and J.-L. Cambier, "Complexity reduction of collisional-radiative kinetics for atomic plasma," *Physics of Plasmas*, vol. 20, no. 12, p. 123304, 2013.

[17] A. Guy, A. Bourdon, and M.-Y. Perrin, "Consistent multi-internal-temperatures models for nonequilibrium nozzle flows," *Chemical Physics*, vol. 420, pp. 15–24, 2013.

[18] A. Guy, A. Bourdon, and M.-Y. Perrin, "Consistent multi-internal-temperature models for vibrational and electronic nonequilibrium in hypersonic nitrogen plasma flows," *Physics of*

Plasmas, vol. 22, no. 4, p. 043507, 2015.

[19] M. Moisan and Z. Zakrzewski, "Plasma sources based on the propagation of electromagnetic surface waves," *Journal of Physics D: Applied Physics*, vol. 24, no. 7, pp. 1025–1048, 1991.

[20] H. Schluter and A. Shivarova, "Travelling-wave-sustained discharges," *Physics Reports*, vol. 443, pp. 121–255, may 2007.

[21] Y. Kabouzi, D. Graves, E. Castaños-Martínez, and M. Moisan, "Modeling of atmospheric-pressure plasma columns sustained by surface waves," *Physical Review E*, vol. 75, p. 016402, jan 2007.

[22] "S. Pancheshnyi, B. Eismann, G.J.M. Hagelaar, L.C. Pitchford, Computer code ZDPlasKin, http://www.zdplaskin.laplace.univ-tlse.fr (University of Toulouse, LAPLACE, CNRS-UPS-INP, Toulouse, France, 2008).."

[23] "Phelps database www.lxcat.net, retrieved on december 4, 2015.."

[24] I. Suzuki, "General anharmonic force constants of carbon dioxide," *Journal of Molecular Spectroscopy*, vol. 25, pp. 479–500, apr 1968.

[25] G. J. M. Hagelaar and L. C. Pitchford, "Solving the Boltzmann equation to obtain electron transport coefficients and rate coefficients for fluid models," *Plasma Sources Science and Technology*, vol. 14, pp. 722–733, nov 2005.

[26] A. Bogaerts, T. Kozák, K. van Laer, and R. Snoeckx, "Plasma-based conversion of CO_2: current status and future challenges," *Faraday Discuss.*, vol. 183, pp. 217–232, 2015.

[27] C. E. Treanor, J. W. Rich, and R. G. Rehm, "Vibrational relaxation of anharmonic oscillators with exchange-dominated collisions," *The Journal of Chemical Physics*, vol. 48, no. 4, pp. 1798–1807, 1968.

[28] L. D. Pietanza, G. Colonna, G. D'Ammando, A. Laricchiuta, and M. Capitelli, "Electron energy distribution functions and fractional power transfer in "cold" and excited co_2 discharge and post discharge conditions," *Physics of Plasmas*, vol. 23, no. 1, 2016.

[29] L. Pietanza, G. Colonna, G. D'Ammando, A. Laricchiuta, and M. Capitelli, "Non equilibrium vibrational assisted dissociation and ionization mechanisms in cold co_2 plasmas," *Chemical Physics*, vol. 468, pp. 44 – 52, 2016.

[30] M. Jimenez-Diaz, E. a. D. Carbone, J. van Dijk, and J. J. a. M. van der Mullen, "A two-dimensional Plasimo multiphysics model for the plasma-electromagnetic interaction in surface wave discharges: the surfatron source," *Journal of Physics D: Applied Physics*, vol. 45, p. 335204, aug 2012.

[31] Y. Itikawa, "Cross Sections for Electron Collisions With Carbon Dioxide," *Journal of Physical and Chemical Reference Data*, vol. 31, no. 3, p. 749, 2002.

[32] M. Hayashi, "Electron collision cross-sections determined from beam and swarm data by boltzmann analysis," in *Nonequilibrium Processes in Partially Ionized Gases* (M. Capitelli and J. Bardsley, eds.), vol. 220 of *NATO ASI Series*, pp. 333–340, Springer US, 1990.

[33] J. E. Land, "Electron scattering cross sections for momentum transfer and inelastic excitation in carbon monoxide," *Journal of Applied Physics*, vol. 49, no. 12, pp. 5716–5721, 1978.

[34] "Morgan database, www.lxcat.net, retrieved on december 4, 2015.."

[35] H. Hokazono and H. Fujimoto, "Theoretical analysis of the CO_2 molecule decomposition and contaminants yield in transversely excited atmospheric CO_2 laser discharge," *Journal of Applied Physics*, vol. 62, no. 5, p. 1585, 1987.

[36] T. G. Beuthe and J.-S. Chang, "Chemical Kinetic Modelling of Non-Equilibrium Ar-CO_2 Thermal Plasmas," *Japanese Journal of Applied Physics*, vol. 36, no. Part 1, No. 7B, pp. 4997–5002, 1997.

[37] A. Cenian, A. Chernukho, V. Borodin, and G. Sliwinski, "Modeling of Plasma-Chemical Reactions in Gas mixture of CO_2 Lasers I. Gas Decomposition in Pure CO_2 Glow Discharge," *Contrib. Plasma Phys.*, vol. 34, pp. 25–37, 1994.

[38] J. T. Gudmundsson and E. G. Thorsteinsson, "Oxygen discharges diluted with argon: dissociation processes," *Plasma Sources Science and Technology*, vol. 16, no. 2, pp. 399–412, 2007.

[39] A. Cenian, A. Chernukho, and V. Borodin, "Modeling of Plasma-Chemical Reactions in Gas Mixture of CO_2 lasers. II. Theoretical Model and its Verification," *Contributions to Plasma*

Physics, vol. 35, pp. 273–296, 1995.

[40] B. Eliasson, M. Hirth, and U. Kogelschatz, "Ozone synthesis from oxygen in dielectric barrier discharges," *Journal of Physics D: Applied Physics*, vol. 20, no. 11, pp. 1421–1437, 1987.

[41] J. A. Blauer and G. R. Gilmore, "A survey of vibrational relaxation rate data for processes important to CO_2-N_2-H_2O infrared plume radiation," *Ultrasystems, Inc. Technical Report*, pp. afrpl–tr–7, 1973.

[42] R. D. Sharma, "Near Resonant Vibrational Energy Transfer among Isotopes of CO_2," *Physical Review*, vol. 177, no. 5, pp. 102–107, 1969.

[43] T. G. Kreutz, J. A. O'Neill, and G. W. Flynn, "Diode Laser Absorption Probe of Vibration-Vibration Energy Transfer in CO_2," *The Journal of Physical Chemistry*, vol. 91, no. 22, pp. 5540–5543, 1987.

[44] H.-j. Mick, M. Burmeister, and P. Roth, "Atomic Resonance Absorption Spectroscopy Measurements on High-Temperature CO Dissociation Kinetics," *AIAA Journal*, vol. 31, no. 4, pp. 671–676, 1993.

[45] S. Hadj-Ziane, B. Held, P. Pignolet, R. Peyrous, and C. Coste, "Ozone generation in an oxygen-fed wire-to-cylinder ozonizer at atmospheric pressure," *Journal of Physics D: Applied Physics*, vol. 25, no. 4, p. 677, 1992.